ATLAS NOTE

ATLAS-CONF-2013-061

25 June, 2013
Revision: 19 August, 2013

Search for strong production of supersymmetric particles in final states with missing transverse momentum and at least three b-jets using 20.1 fb^{-1} of pp collisions at $\sqrt{s}$ = 8 TeV with the ATLAS Detector.

The ATLAS Collaboration

Abstract

The results of a search for strong production of supersymmetric particles in multi-b-jets final states in 20.1 fb^{-1} of pp collisions at $\sqrt{s} = 8$ TeV using the ATLAS detector at the LHC are reported. This search is performed in events with zero or at least one lepton (electron or muon), large missing transverse momentum, at least four, six or seven jets and at least three jets tagged as originating from b-quarks. No excess is observed in data with respect to the Standard Model predictions. Results are interpreted in the context of several supersymmetric models involving gluinos and top and bottom squarks, and in the context of a mSUGRA/CMSSM model. Gluino masses up to about 1.3 TeV are excluded, depending on the model, which significantly extends the previous ATLAS results.

ATLAS-CONF-2013-061
25/08/2013

A typo was found in some labels in Tables 6 and 8 in the Appendix, where $m_{\mathrm{eff}}^{\mathrm{incl}}$ has been replaced by $m_{\mathrm{eff}}^{\mathrm{4j}}$ (Table 6), and m_{eff} and $E_{\mathrm{T}}^{\mathrm{miss}}/\sqrt{H_T}$ have been replaced by $m_{\mathrm{eff}}^{\mathrm{incl}}$ and $E_{\mathrm{T}}^{\mathrm{miss}}/\sqrt{H_{\mathrm{T}}^{\mathrm{incl}}}$ (Table 8), respectively. None of the corresponding numbers have been changed.

1 Introduction

Supersymmetry (SUSY) [1–9] provides an extension of the Standard Model (SM) which solves the hierarchy problem [10–13] by introducing supersymmetric partners for SM particles. In the framework of the *R*-parity conserving minimal supersymmetric extension of the SM (MSSM) [14–18], SUSY particles are produced in pairs and the lightest supersymmetric particle (LSP) is stable. In a large variety of models, the LSP is the lightest neutralino[1] ($\tilde{\chi}_1^0$), which is weakly interacting, thus providing a possible candidate for dark matter. The coloured superpartners of quarks and gluons, the squarks ($\tilde{q}$) and gluinos ($\tilde{g}$), if not too heavy, would be produced in strong interaction processes at the Large Hadron Collider (LHC) and decay via cascades ending with the LSP. The undetected LSP results in missing transverse momentum – whose magnitude is referred to as $E_{\mathrm{T}}^{\mathrm{miss}}$ – while the rest of the cascade yields final states with multiple jets and possibly leptons. The scalar partners of the right-handed and left-handed quarks, $\tilde{q}_R$ and $\tilde{q}_L$, mix to form two mass eigenstates $\tilde{q}_1$ and $\tilde{q}_2$, with a mixing effect that is proportional to the masses of the SM fermion partners. SUSY can naturally solve the hierarchy problem, by preventing "unnatural" fine-tuning in the Higgs sector, provided that the superpartners of the top quark ($\tilde{t}$, stop) have masses not too far above the weak scale [19,20]. This condition requires that the gluino is not too heavy due to its contribution to the radiative corrections to the stop masses. The constraint on the stop masses also implies that the left-handed sbottom ($\tilde{b}_L$) is expected to be relatively light because of the SM weak isospin symmetry. As a consequence, the lightest sbottom ($\tilde{b}_1$) and stop ($\tilde{t}_1$) could be produced with relatively large cross-sections at the LHC, either directly in pairs, or through $\tilde{g}\tilde{g}$ production followed by $\tilde{g} \to \tilde{b}_1 b$ or $\tilde{g} \to \tilde{t}_1 t$ decays.

This note extends the search for gluino pair production in final states with at least three jets identified as originating from *b*-quarks (*b*-jets) at ATLAS [21], which used 12.8 fb^{-1} of data collected in 2012 at a centre-of-mass energy of 8 TeV. A first version of this analysis was performed with the full data set recorded by the ATLAS detector in 2011 at $\sqrt{s}$=7 TeV [22]. Both these analyses used events with no electrons or muons (0-lepton), large $E_{\mathrm{T}}^{\mathrm{miss}}$ and at least three *b*-jets in the final state. The present analysis uses the dataset of 20.1 fb^{-1} collected during 2012 at a centre-of-mass energy of 8 TeV and extends the previous analyses by adding final states with at least one electron or one muon (1-lepton). The results are interpreted in the context of various SUSY models where top or bottom quarks are produced in gluino decay chains. Additional interpretations are provided for a direct sbottom pair production scenario where the sbottom decays into a bottom quark and the next-to-lightest neutralino, $\tilde{\chi}_2^0$, followed by the $\tilde{\chi}_2^0$ decay into a Higgs boson and the LSP, and for a mSUGRA/CMSSM model designed to accommodate a Higgs boson with a mass of about 125 GeV. Exclusion limits in similar SUSY models have also been placed by several analyses carried out by the ATLAS [23–25] and CMS [26,27] collaborations with the same integrated luminosity at 8 TeV.

2 SUSY signals

Several classes of models are used for the optimisation of the event selection and interpretation of the results. Results from the 0-lepton channel are used to explore all models considered, while the complementarity between the searches in the 0- and 1-lepton channels is used to maximise the sensitivity to models predicting Higgs bosons or top quarks in the final state.

In the first class of simplified models, the lightest stops and sbottoms are lighter than the

[1] The SUSY partners of the electroweak gauge and Higgs bosons are called gauginos and higgsinos, respectively. The charged gauginos and higgsinos mix to charginos ($\tilde{\chi}^{\pm}$), and the neutral ones mix to neutralinos ($\tilde{\chi}^0$).

gluino, such that $\tilde{b}_1$ and $\tilde{t}_1$ are produced either in pairs, or via gluino pair production followed by $\tilde{g} \to \tilde{b}_1 b$ or $\tilde{g} \to \tilde{t}_1 t$ decays. The mass of the neutralino[2] is set at 60 GeV consistently for all these models. They are described in detail in the following :

In the **Direct-Sbottom model**, the $\tilde{b}_1$ is produced in pairs and is assumed to decay exclusively via $\tilde{b}_1 \to b + \tilde{\chi}_2^0$. In scenarios where slepton masses are set above few TeV, the $\tilde{\chi}_2^0$ decays via an off-shell or on-shell Higgs or Z boson. The mass of the lightest neutral Higgs boson (h) is set to 125 GeV, and its decay branching ratios are assumed to be those of the SM Higgs boson. In this analysis, only the configuration $m_{\tilde{\chi}_2^0} > m_{\tilde{\chi}_1^0} + m_h$ is considered, with a branching ratio for $\tilde{\chi}_2^0 \to h + \tilde{\chi}_1^0$ of 100%. This analysis is mainly sensitive to signal events where both Higgs bosons decay into a $b\bar{b}$ pair, yielding a signature with no lepton, six bottom quarks and large $E_{\mathrm{T}}^{\mathrm{miss}}$. A small sensitivity is also obtained in the 1-lepton channel for events where one Higgs boson decays into a $b\bar{b}$ pair, while the other one decays into W^+W^- followed by the hadronic decay of one W-boson and the leptonic decay of the second one. Exclusion limits are presented in the $(m_{\tilde{b}_1}, m_{\tilde{\chi}_2^0})$ plane.

In the **Gluino-Sbottom model**, the $\tilde{b}_1$ is the lightest squark, all other squarks are heavier than the gluino, and $m_{\tilde{g}} > m_{\tilde{b}_1} + m_b$ such that the branching ratio for $\tilde{g} \to \tilde{b}_1 b$ decays is 100%. Sbottoms are produced in pairs or via gluino pair production and are assumed to decay exclusively via $\tilde{b}_1 \to b\tilde{\chi}_1^0$. This analysis is only sensitive to the gluino mediated production where final states contain four bottom quarks and two neutralinos. Exclusion limits are presented in the $(m_{\tilde{g}}, m_{\tilde{b}_1})$ plane.

In the **Gluino-Stop I model**, the $\tilde{t}_1$ is the lightest squark, all other squarks are heavier than the gluino, and $m_{\tilde{g}} > m_{\tilde{t}_1} + m_t$ such that the branching ratio for $\tilde{g} \to \tilde{t}_1 t$ decays is 100%. Stops are produced in pairs or via gluino pair production and are assumed to decay exclusively via $\tilde{t}_1 \to b\tilde{\chi}_1^{\pm}$. The chargino mass is assumed to be twice the mass of the neutralino, such that the chargino decays into a neutralino and a virtual W boson. This analysis is only sensitive to the gluino mediated production where the final state contains two top quarks, two bottom quarks, two virtual W-bosons and two neutralinos, yielding signatures with or without leptons. Exclusion limits are presented in the $(m_{\tilde{g}}, m_{\tilde{t}_1})$ plane.

The **Gluino-Stop II model** is identical to the Gluino-Stop I model, except that the stops are assumed to decay exclusively via $\tilde{t}_1 \to t\tilde{\chi}_1^0$. The final state contains four top quarks and two neutralinos, yielding signatures with or without leptons. Exclusion limits are presented in the $(m_{\tilde{g}}, m_{\tilde{t}_1})$ plane.

In the second class of simplified models, all sparticles, apart from the gluino and the neutralino, are well above the TeV scale such that the $\tilde{t}_1$ and the $\tilde{b}_1$ are only produced off-shell via gluino pair production. The sbottom and stop masses have no impact on the kinematic of the final state and the exclusion limits are presented in the $(m_{\tilde{g}}, m_{\tilde{\chi}_1^0})$ plane. These models are described in detail in the following :

In the **Gbb model**, the $\tilde{b}_1$ is the lightest squark, but with $m_{\tilde{g}} < m_{\tilde{b}_1}$. A three-body decay via an off-shell sbottom is assumed for the gluino, yielding a branching ratio of 100% for the decay $\tilde{g} \to b\bar{b}\tilde{\chi}_1^0$. As for the Gluino-Sbottom model, the final state contains only four bottom quarks and two neutralinos.

In the **Gtt model**, the $\tilde{t}_1$ is the lightest squark, but $m_{\tilde{g}} < m_{\tilde{t}_1}$. A three-body decay via an off-shell stop is assumed for the gluino, yielding a branching ratio of 100% for the decay $\tilde{g} \to t\bar{t}\tilde{\chi}_1^0$.

[2]Here and in the rest of this note, neutralino is to be understood as lightest neutralino.

The final state contains four top quarks and two neutralinos, resulting in signatures with or without leptons.

In the **Gtb model**, the $\tilde{b}_1$ and $\tilde{t}_1$ are the lightest squarks but $m_{\tilde{g}} < m_{\tilde{b}_1,\tilde{t}_1}$. Pair production of gluinos is the only process taken into account, with gluinos decaying via virtual stops or sbottoms with a branching ratio of 100% assumed for $\tilde{t}_1 \to b + \tilde{\chi}_1^{\pm}$ and $\tilde{b}_1 \to t + \tilde{\chi}_1^{\pm}$, respectively. The mass difference between charginos and neutralinos is set to 2 GeV, such that the fermions produced in $\tilde{\chi}_1^{\pm} \to \tilde{\chi}_1^0 + ff'$ are invisible to the event selection, and gluino decays result in effectively three-body final states ($b\bar{t}\tilde{\chi}_1^0$ or $t\bar{b}\tilde{\chi}_1^0$). The event final state contains two top quarks, two bottom quarks and two neutralinos, yielding signatures with or without leptons.

Finally, all results are also interpreted in the context of a minimal supergravity model **mSUGRA/CMSSM** specified by five parameters: the universal scalar mass m_0, the universal gaugino mass $m_{\frac{1}{2}}$, the universal trilinear scalar coupling A_0, the ratio of the vacuum expectation values of the two Higgs fields $\tan\beta$, and the sign of the higgsino mass parameter μ. The model used for interpretation is designed to accommodate a SM Higgs boson with a mass of around 125 GeV. The results are presented in the (m_0, $m_{\frac{1}{2}}$) plane, with the other parameters set as : $\tan\beta$=30, $A_0 = -2m_0$ and $\mu > 0$.

3 The ATLAS detector

The ATLAS detector [28] consists of inner tracking devices surrounded by a superconducting solenoid, electromagnetic and hadronic calorimeters and a muon spectrometer with three large superconducting air-core toroid magnets. The inner detector, in combination with the 2 T field from the solenoid, provides precision tracking of charged particles for $|\eta| < 2.5$[3]. It consists of a silicon pixel detector, a silicon strip detector and a straw tube tracker that also provides transition radiation measurements for electron identification. The calorimeter system covers the pseudo-rapidity range $|\eta| < 4.9$. It is composed of sampling calorimeters with either liquid argon (LAr) or scintillating tiles as the active medium. The muon spectrometer has separate trigger and high-precision tracking chambers which provide muon identification and momentum measurement for $|\eta| < 2.7$.

4 Monte Carlo simulation

Samples of simulated Monte Carlo (MC) events are used to assess the sensitivity to specific SUSY models and aid in the prediction of the different SM background contributions. The various background processes are divided into two categories in the analysis depending on whether they lead to final states with at least three real b-jets (irreducible) or not (reducible). Irreducible backgrounds arise from $t\bar{t}$ + b and $t\bar{t}$ + $b\bar{b}$ production, and from $t\bar{t}$+Z/h, with $Z/h \to b\bar{b}$. Background contributions from events where at least one b-jet is misidentified as a b-jet are classified as reducible and arise from $t\bar{t}$ production in association with light flavour jets, single top quark production, W/Z+jets production, and diboson (WW, WZ, ZZ) production. In this analysis, only the irreducible backgrounds are estimated from MC simulations, while the

[3] ATLAS uses a right-handed coordinate system with its origin at the nominal interaction point (IP) in the centre of the detector and the z-axis along the beam pipe. The x-axis points from the IP to the centre of the LHC ring, and the y axis points upward. Cylindrical coordinates (r,ϕ) are used in the transverse plane, ϕ being the azimuthal angle around the beam pipe. The pseudo-rapidity is defined in terms of the polar angle θ as $\eta = -\ln\tan(\theta/2)$.The distance ΔR in the $\eta - \phi$ space is defined as $\Delta R = \sqrt{(\Delta\eta)^2 + (\Delta\phi)^2}$.

reducible backgrounds are estimated using a data-driven method. MC samples are used to validate the prediction of the data-driven method for all reducible backgrounds.

Samples of $t\bar{t}$ events are generated using POWHEG-BOX 1.0 [29] interfaced to PYTHIA 6.426 [30] with the P2011C tune [31] and the Next-to-Leading Order (NLO) parton distribution function (PDF) set CT10 [32]. The distinction between the reducible background $t\bar{t}$ + jets and the irreducible backgrounds $t\bar{t}$ + b and $t\bar{t}$ + $b\bar{b}$ is performed by matching the jets to b-quarks. Single top production is generated using AcerMC 3.8 [33] interfaced to PYTHIA6 and the PDF set CTEQ6L1 [34] for the t-channel, and using MC@NLO 4.06 [35] interfaced to HERWIG 6.520 [36] and JIMMY 4.31 [37] with the PDF set CT10 for the s-channel and Wt processes. The W and Z events produced in association with light- and heavy-flavour jets are generated with SHERPA 1.4.1 [38] with up to four additional partons in the matrix element, treating b-quarks and c-quarks as massive in the calculation, and using the PDF set CT10. Diboson events are generated with up to three additional partons in the matrix element using SHERPA and the PDF set CT10. Samples of $t\bar{t}$+W and $t\bar{t}$+Z events with up to two additional partons are generated with MADGRAPH 5.1.4.8 [39] interfaced to PYTHIA6 and with the PDF set CTEQ6L1. Simulated samples of Higgs boson produced in association with a pair of top quarks and decaying into a pair of bottom quarks are generated with PYTHIA 8.1 [40] and the PDF set CTEQ6L1 for a Higgs boson mass of 125 GeV.

The signal samples for the Gbb model are generated with MADGRAPH [39] interfaced to PYTHIA6 in order to ensure an accurate treatment of the initial-state radiation (ISR), and with the PDF set CTEQ6L1. All other signal samples are generated using HERWIG++ 2.5.2 [41] and the PDF set CTEQ6L1.

For the comparison with data, all SM background cross-sections are normalised to the results of higher-order calculations. Signal cross-sections are calculated to next-to-leading order in the strong coupling constant, adding the re-summation of soft gluon emission at next-to-leading-logarithmic accuracy (NLO+NLL) [42–46]. The nominal cross-section and the uncertainty $\sigma^{\text{SUSY}}_{\text{Theory}}$ are taken from an envelope of cross-section predictions using different PDF sets and factorisation and renormalisation scales, as prescribed in Ref. [47].

The MC samples are processed either through a full simulation [48] of the ATLAS detector based on GEANT4 [49] or a fast simulation [50] based on a parameterisation of the performance of the ATLAS electromagnetic and hadronic calorimeters. The effect of multiple pp interactions per bunch crossing is taken into account in the simulation.

5 Object reconstruction

Jets are reconstructed from three-dimensional calorimeter energy clusters using the anti-k_t jet algorithm [51, 52] with a distance parameter of 0.4. The measured jet energy is corrected for inhomogeneities and for the non-compensating nature of the calorimeter by weighting differently energy deposits arising from electromagnetic and hadronic showers using correction factors derived from Monte Carlo simulations and validated with data [53]. The jets are corrected for energy from additional proton-proton collisions in the same or neighbouring bunch crossings (pile-up) using a method, suggested in Ref. [54], which estimates the pile-up activity in any given event, as well as the sensitivity of any given jet to pile-up. The method subtracts a contribution from the jet energy equal to the product of the jet area and the event average energy density. The residual impact of additional collisions in the same or neighbouring bunch crossings is taken into account using corrections derived as a function of the average number of interactions per bunch crossing $< \mu >$ and of the number of primary vertices N_{PV}. Finally, additional corrections are applied to calibrate the energies of jets to the mean scale of their con-

stituent particles. Only jets with $|\eta| < 4.5$ and $p_{\mathrm{T}} > 20$ GeV after calibration are retained. Events are rejected if they include jets failing the quality criteria described in Ref. [53]. To further reject spurious jet signals, additional criteria are applied on the charged p_{T} fraction f_{ch}, defined as the fraction of the transverse momentum of the jet carried by charged tracks, and on the fraction of the jet energy contained in the electromagnetic layers of the calorimeter f_{em}. Events are rejected if either of the two leading jets with $p_{\mathrm{T}} > 100$ GeV and $|\eta| < 2.0$ satisfies $f_{\mathrm{ch}} < 0.02$ or $f_{\mathrm{ch}} < 0.05$ and $f_{\mathrm{em}} > 0.9$. Except during the $E_{\mathrm{T}}^{\mathrm{miss}}$ computation, only jets with $|\eta| < 2.8$ are further considered.

A neural-network-based algorithm [55] is used to identify jets containing a b-hadron decay. This uses as inputs the output weights of different algorithms exploiting the impact parameter of the inner detector tracks, the secondary vertex reconstruction and the topology of b-and c-hadron decays inside the jet. The algorithm used has an efficiency of 70% for tagging b-jets in a MC sample of $t\bar{t}$ events with rejection factors of 137, 5 and 13 against light quarks, c-quarks and τ leptons respectively. The b-jets are identified within the nominal acceptance of the inner detector ($|\eta| < 2.5$). To compensate for the differences between the b-tagging efficiencies and the misidentification (mistag) rates in data and MC simulation, scale factors are applied to each jet in the simulations, as described in Refs. [55–57]. These corrections are of the order of few percent.

Electrons are reconstructed from energy clusters in the electromagnetic calorimeter associated to tracks in the inner detector. Two classes of electrons are defined: baseline electron candidates are required to have $p_{\mathrm{T}} > 20$ GeV and $|\eta| < 2.47$ and must satisfy the *medium++* shower shape and track selection criteria described in Ref. [58]. Signal electrons must satisfy more stringent quality requirements, denoted by *tight++* in Ref. [58], and be isolated, i.e. the total p_{T} of additional charged particles or calorimeter energy inside a cone of radius $\Delta R = 0.2$ around the electron must be smaller than 16% and 18%, respectively, of the electron p_{T}. In addition, the charged track assigned to the electron candidate must have a longitudinal impact parameter defined with respect to the primary vertex z_0 satisfying $|z_0 \sin\theta| < 0.4$ mm and a transverse impact parameter d_0 within $3\sigma(d_0)$.

Muon candidates are identified using a match between an extrapolated inner detector track and one or more track segments in the muon spectrometer. Two classes of muons are defined: baseline muons are required to have $p_{\mathrm{T}} > 10$ GeV and $|\eta| < 2.4$. Signal muons must have $p_{\mathrm{T}} > 20$ GeVand be isolated, following the same criteria used for electrons, but with isolation cuts of 12% of the muon momentum. The same impact parameter requirements as for electrons are applied.

To resolve overlaps between reconstructed jets and leptons, jets within a distance of $\Delta R = 0.2$ of a baseline electron candidate are rejected. Furthermore, any baseline lepton candidate with a distance $\Delta R < 0.4$ to the closest remaining jet is discarded.

The measurement of the missing transverse momentum two-dimensional vector (and its magnitude $E_{\mathrm{T}}^{\mathrm{miss}}$) is based on the transverse momenta of all jets, electron and muon candidates and all calorimeter cells not associated to such objects. Clusters associated to either electrons or photons with $p_{\mathrm{T}} > 10$ GeV, and those associated with jets with $p_{\mathrm{T}} > 20$ GeV, make use of the calibrations of these respective objects. Clusters not associated with these objects are calibrated using both calorimeter and tracker information.

6 Event selection

Events are selected using a logical OR of two triggers based on $E_{\mathrm{T}}^{\mathrm{miss}}$. These triggers are fully efficient for both the 0-lepton and 1-lepton analyses which require at least one jet with $p_{\mathrm{T}} >$

90 GeV and $E_{\mathrm{T}}^{\mathrm{miss}} > 150$ GeV at the offline reconstruction stage. After the trigger selection, events must pass basic quality criteria to reject detector noise and non-collision backgrounds. They are also required to have a reconstructed primary vertex associated with five or more tracks with $p_{\mathrm{T}} > 0.4$ GeV; when more than one such vertex is found, the vertex with the largest summed p_{T}^2 of the associated tracks is chosen as the primary vertex. Events are required to have at least four jets with $p_{\mathrm{T}} > 30$ GeV, at least three b-tagged jets with $p_{\mathrm{T}} > 30$ GeV, and are divided into two categories based on the number of leptons: events containing any remaining baseline electrons or muons are vetoed in the 0-lepton channel; for the 1-lepton channel, only events with at least one signal lepton are considered.

The events are further classified in various "signal regions", each defined by a set of selection criteria that make use of several variables calculated from the reconstructed objects. For the 0-lepton channel, four additional variables, described below, are used.

- The inclusive effective mass $m_{\mathrm{eff}}^{\mathrm{incl}}$, defined as the scalar sum of the $E_{\mathrm{T}}^{\mathrm{miss}}$ and the p_{T} of all jets with $p_{\mathrm{T}} > 30$ GeV, is correlated with the overall mass scale of the hard-scattering and provides good discrimination against SM background.

- The exclusive effective mass $m_{\mathrm{eff}}^{\mathrm{4j}}$ is defined as the scalar sum of the $E_{\mathrm{T}}^{\mathrm{miss}}$ and the p_{T} of the four leading jets. It is used to suppress the multi-jet background and to define the signal regions targeting SUSY signals where exactly four b-jets and large $E_{\mathrm{T}}^{\mathrm{miss}}$ are expected in the final state.

- The $\Delta\phi_{\mathrm{min}}^{4j}$ is defined as the minimum azimuthal separation between any of the four leading jets and the missing transverse momentum direction. To remove multi-jet events, where $E_{\mathrm{T}}^{\mathrm{miss}}$ results from mis-reconstructed jets or from neutrinos emitted close to the direction of the jet axis, events are required to have $\Delta\phi_{\mathrm{min}}^{4j} > 0.5$ and $E_{\mathrm{T}}^{\mathrm{miss}}/m_{\mathrm{eff}}^{\mathrm{4j}} > 0.2$. The combination of these two requirements reduces the contribution of the multi-jet background to a negligible amount.

- The missing transverse momentum significance, defined as the ratio of the $E_{\mathrm{T}}^{\mathrm{miss}}$ to the square root of the scalar sum $H_{\mathrm{T}}^{\mathrm{4j}}$ of the transverse momenta of the four leading jets, $E_{\mathrm{T}}^{\mathrm{miss}}/\sqrt{H_{\mathrm{T}}^{\mathrm{4j}}}$, is used to define the signal regions aiming at SUSY signals with four jets in the final state.

For the 1-lepton channel, event selections are defined using similarly constructed variables, but also taking into account the leading lepton p_{T}.

- $m_{\mathrm{eff}}^{\mathrm{incl}}$, defined as for the 0-lepton channel with the addition of the p_{T} of the leading lepton.

- $E_{\mathrm{T}}^{\mathrm{miss}}/\sqrt{H_{\mathrm{T}}^{\mathrm{incl}}}$, where $H_{\mathrm{T}}^{\mathrm{incl}}$ is the scalar sum of the transverse momenta of all jets with $p_{\mathrm{T}} > 30$ GeV and the p_{T} of the leading lepton.

- The transverse mass m_{T} computed from the leading lepton and the missing transverse momentum as $m_{\mathrm{T}} = \sqrt{2p_{\mathrm{T}}E_{\mathrm{T}}^{\mathrm{miss}}(1-\cos\Delta\phi(\ell, E_{\mathrm{T}}^{\mathrm{miss}}))}$, used to reject the main background coming from $t\bar{t}$ events where one of the W bosons decays leptonically. After the m_{T} requirement, the dominant contribution to the $t\bar{t}$ background arises from dileptonic $t\bar{t}$ events.

Three sets of signal regions, two for the 0-lepton channel and one for the 1-lepton channel, are defined to enhance the sensitivity to the various models considered. They are characterised by having relatively hard $E_{\mathrm{T}}^{\mathrm{miss}}$ requirements and at least four (SR-0l-4j), six (SR-1l-6j) or seven (SR-0l-7j) jets, amongst which at least three are b-tagged jets. They are further classified as A/B/C depending on the thresholds applied to the various variables defined above. Additional validation regions (VR) with low expected signal contribution are used to verify the background predictions. The requirements that characterise all validation and signal regions are summarised in Tables 1 and 2 for the 0- and 1-lepton channels, respectively.

baseline selection: baseline lepton veto, $p_T^{j_1} > 90$ GeV, $E_{\mathrm{T}}^{\mathrm{miss}} > 150$ GeV, ≥ 4 jets with $p_T > 30$ GeV, $\Delta\phi_{\mathrm{min}}^{4j} > 0.5$, $E_{\mathrm{T}}^{\mathrm{miss}}/m_{\mathrm{eff}}^{4\mathrm{j}} > 0.2$, ≥ 3 b-jets with $p_T > 30$ GeV					
0-ℓ region	N jets	p_T jets [GeV]	$E_{\mathrm{T}}^{\mathrm{miss}}$ [GeV]	m_{eff} [GeV]	$E_{\mathrm{T}}^{\mathrm{miss}}/\sqrt{H_{\mathrm{T}}^{4\mathrm{j}}}$ [GeV$^{\frac{1}{2}}$]
VR-0l-4j-A	≥ 4	> 30	> 150	-	< 16
VR-0l-4j-B	≥ 4	> 50	> 150	$m_{\mathrm{eff}}^{4\mathrm{j}} < 1000$	-
VR-0l-7j-A	≥ 7	> 30	> 150	$m_{\mathrm{eff}}^{\mathrm{incl}} < 1000$	-
VR-0l-7j-B	≥ 7	> 30	$150 < E_{\mathrm{T}}^{\mathrm{miss}} < 350$	$m_{\mathrm{eff}}^{\mathrm{incl}} < 1500$	-
SR-0l-4j-A	≥ 4	> 30	> 200	$m_{\mathrm{eff}}^{4\mathrm{j}} > 1000$	> 16
SR-0l-4j-B	≥ 4	> 50	> 350	$m_{\mathrm{eff}}^{4\mathrm{j}} > 1100$	-
SR-0l-4j-C	≥ 4	> 50	> 250	$m_{\mathrm{eff}}^{4\mathrm{j}} > 1300$	-
SR-0l-7j-A	≥ 7	> 30	> 200	$m_{\mathrm{eff}}^{\mathrm{incl}} > 1000$	-
SR-0l-7j-B	≥ 7	> 30	> 350	$m_{\mathrm{eff}}^{\mathrm{incl}} > 1000$	-
SR-0l-7j-C	≥ 7	> 30	> 250	$m_{\mathrm{eff}}^{\mathrm{incl}} > 1500$	-

Table 1: Definition of all validation and signal regions used in the 0-lepton analysis, based on the number of jets with $p_{\mathrm{T}} > 30$ GeV or $p_{\mathrm{T}} > 50$ GeV, the jets and b-jets p_{T} thresholds, the missing transverse momentum, the effective mass, and the missing transverse momentum significance.

baseline selection: $\geqslant 1$ signal lepton (e,μ), $p_T^{j_1} > 90$ GeV, $E_{\mathrm{T}}^{\mathrm{miss}} > 150$ GeV, ≥ 4 jets with $p_T > 30$ GeV, ≥ 3 b-jets with $p_T > 30$ GeV					
1-ℓ region	N jets	$E_{\mathrm{T}}^{\mathrm{miss}}$ [GeV]	m_{T} [GeV]	$m_{\mathrm{eff}}^{\mathrm{incl}}$ [GeV]	$E_{\mathrm{T}}^{\mathrm{miss}}/\sqrt{H_{\mathrm{T}}^{\mathrm{incl}}}$ [GeV$^{\frac{1}{2}}$]
VR-1l-4j	≥ 4	> 150	> 100	-	-
VR-1l-6j	≥ 6	> 150	$100 < m_{\mathrm{T}} < 140$	> 600	> 5
SR-1l-6j-A	≥ 6	> 175	> 140	> 700	> 5
SR-1l-6j-B	≥ 6	> 225	> 140	> 800	> 5
SR-1l-6j-C	≥ 6	> 275	> 160	> 900	> 5

Table 2: Definition of all validation and signal regions used in the 1-lepton analysis, based on the number of jets with $p_{\mathrm{T}} > 30$ GeV, the missing transverse momentum, the transverse mass, the effective mass and the missing transverse momentum significance.

7 Background estimate

The main source of reducible background is the production of $t\bar{t}$ events in association with additional non-b jets, where a c-jet or a τ-lepton decaying to hadrons and a ν_τ is mistagged as a b-jet. The contribution from $t\bar{t}$ events with a light or gluon jet mistagged as a b-jet is subdominant. In the 0-lepton channel, most of these $t\bar{t}$ events have a W boson decaying leptonically where the lepton is not reconstructed, is outside of acceptance, is mis-identified as a jet or is a τ which decays hadronically. In the 1-lepton channel, the high m_{T} requirement enhances the contribution from $t\bar{t}$ events with a dilepton final state. Additional sources of reducible background are single top production, $t\bar{t}$+W/Z, except $t\bar{t}$+Z ($Z \to b\bar{b}$), and W/Z+heavy-flavour jets. The remaining irreducible backgrounds with at least three real b-jets in the final state arise from $t\bar{t}$+$b/b\bar{b}$ and $t\bar{t}$+Z/h followed by the decay of the Z or Higgs boson into a pair of b-quarks, and they are extracted from MC simulations.

All reducible background sources are estimated simultaneously using a data-driven method that predicts the contribution from events with at least one mistagged b-jet. This estimate is based on a matrix method (MM) which consists of solving a system of equations based on the number of b-tagged and non b-tagged jets in each event, along with the b-tagging efficiency and mistag rate. The number of b-tagged jets amongst the n-jets of each event is expressed as a linear combination of the number of real and fake b-jets multiplied by the corresponding b-tagging efficiency and mistag rate. For a given event containing n-jets satisfying the η and p_{T} requirements applied for b-tagging jets, 2^n linear equations can be written to take into account all possible combinations of real and fake b-jets. These linear equations are written in the form of a matrix with dimension $2^n \times 2^n$, the mistag rates and b-tagging efficiencies in the matrix corresponding to those of each of the jets in the event, parameterised as a function of the jet p_{T} and η. The system of 2^n equations is solved by inverting the matrix to obtain the probabilities that the event corresponds to each of the possible combinations of real and fake b-jets. An event weight is then calculated by summing these probabilities, taking into account only the combinations with less than three real b-jets. To obtain the reducible background prediction, these weights are applied to each event satisfying all selection criteria, except the b-tagging requirements. The sum of all the weighted events for a given event selection is the total reducible background prediction, which can be binned as a function of any variable to obtain the different variable distributions.

The b-tagging efficiency and mistag rate are measured in data as a function of the jet p_{T} and $|\eta|$. The b-tagging efficiency is measured using a combination of the muon based and $t\bar{t}$ based methods described in Ref. [55] and Ref. [59], respectively. The probability for a given jet to be mistagged depends on the origin of the fake b-jet candidate: light flavour quarks, c-quarks and τ-leptons. Since the origin of a fake b-jet candidate in data is unknown, an average mistag rate which takes into account the relative contribution of each source of fake b-jets is used. The average mistag rates are determined in both $t\bar{t}$ MC simulations and data using 0- and 1-lepton control regions enriched in $t\bar{t}$ events. These control regions are defined as the baseline selection in both channels, except that the b-jets requirements are relaxed to have at least 2 b-jets, and the $E_{\mathrm{T}}^{\mathrm{miss}}$ is required to lie between 100 and 200 GeV in order to minimise the possible contribution from signal events in the data. The mistag rate is measured as the probability to have a third b-jet in bins of p_{T} and η. In the 1-lepton channel, an additional parameterisation in four m_{T} bins is determined to take into account the variation of the $t\bar{t}$ background composition as a function of m_{T}. For the mistag rate measured in data, the contribution from events with at least three real b-jets is subtracted using MC simulations. Because of lack of statistics in data, the mistag rate estimated in the $t\bar{t}$ MC sample is taken as baseline, and the difference between the two

measurements is treated as a systematic uncertainty. The resulting relative uncertainty on the event yield varies between 4% and 20% depending on the signal region considered.

To validate the method, a "closure" test is performed by applying the method directly on the $t\bar{t}$ MC simulation. In the 0-lepton channel, the closure test is done after the baseline selection described in Table 1. In the 1-lepton channel, the closure test is first performed after the 1-lepton baseline selection described in Table 2 to validate the prediction of the jet multiplicity. The prediction is then validated for all other variables after requiring six jets with $p_{\mathrm{T}} > 30$ GeV to match the signal region definitions. The results of the closure test in the 0-lepton (1-lepton) channel for the number of jets with $p_{\mathrm{T}} > 30$ GeV, the leading jet p_{T} (the m_{T}), the $E_{\mathrm{T}}^{\mathrm{miss}}$ and the effective mass distributions are shown in Figure 1 (Figure 2). A reasonable description of the reducible $t\bar{t}$ background is obtained with the matrix method for all kinematic variables used in this analysis.

8 Systematic uncertainties

The dominant detector-related systematic uncertainties are due to the jet energy scale (JES) and resolution (JER) uncertainties, and to the uncertainty in the b-tagging efficiencies which are measured separately for b-, c-, light and τ jets. The JES uncertainty is derived from a combination of simulations, test beam data and in-situ measurements [53, 60]. Additional contributions accounting for the jet flavour composition, the calorimeter response to different jet flavours, pile-up and b-jet calibration uncertainties are taken into account. Uncertainties in the JER are obtained with an in-situ measurement of the jet response asymmetry in di-jet events. Uncertainties on jets are propagated to the $E_{\mathrm{T}}^{\mathrm{miss}}$ measurement, and additional uncertainties on $E_{\mathrm{T}}^{\mathrm{miss}}$ arising from energy deposits not associated with any reconstructed objects are also included. The b-tagging uncertainty is evaluated by varying the η-, p_{T}- and flavour-dependent scale factors applied to each jet in the simulation within a range that reflects the systematic uncertainty on the measured tagging efficiencies and mistag rates. These experimental systematic uncertainties are treated as fully correlated between the signal and the irreducible backgrounds extracted from MC.

Additional theoretical systematic uncertainties are applied to the irreducible backgrounds. Firstly, there are theoretical uncertainties on the $t\bar{t}+b$ and $t\bar{t}+b\bar{b}$ cross sections due to unknown higher order corrections which are considered. The ratio R_{HF} of the cross section for $t\bar{t}$ + heavy-flavour quarks production to the cross section for $t\bar{t}$ production with at least one additional jet has been measured by the ATLAS collaboration in a fiducial kinematic region with the full data set recorded at $\sqrt{s} = 7$ TeV [61]. The measured R_{HF} is 7.1 $\pm$ 1.3 (stat.) $^{+\,5.3}_{-\,2.0}$ (syst.)% for jets with $p_{\mathrm{T}} > 25$ GeV and $|\eta| < 2.5$, which is consistent with R_{HF} of 5.2% obtained using the POWHEG nominal $t\bar{t}$ sample employed in this analysis. A similar measurement has been carried out by the CMS collaboration leading to a consistent result [62]. Since the measured R_{HF} is consistent with POWHEG in the kinematic region used to perform this analysis, no correction factor is applied to the $t\bar{t}+b/b\bar{b}$ yield extracted from MC. However the full uncertainty of the ATLAS measurement of R_{HF} is taken as an uncertainty on the $t\bar{t}+b/b\bar{b}$ cross-section, and the uncertainty on the inclusive $t\bar{t}$ cross-section is added in quadrature. The $t\bar{t}$ cross-section for pp collisions at a centre-of-mass energy of $\sqrt{s} = 8$ TeV is $\sigma_{t\bar{t}} = 238^{+22}_{-24}$ pb for a top quark mass of 172.5 GeV. It has been calculated at approximate NNLO in QCD with Hathor 1.2 [63] using the MSTW2008 NNLO PDF sets [64] incorporating PDF+α_S uncertainties, according to the MSTW prescription [65], added in quadrature to the scale uncertainty and cross checked with the NLO+NNLL calculation of Ref. [66] as implemented in Top++ 1.0 [67]. An uncertainty of 3% on the $t\bar{t}$ cross-section is also added to take into account the uncertainty due to a variation

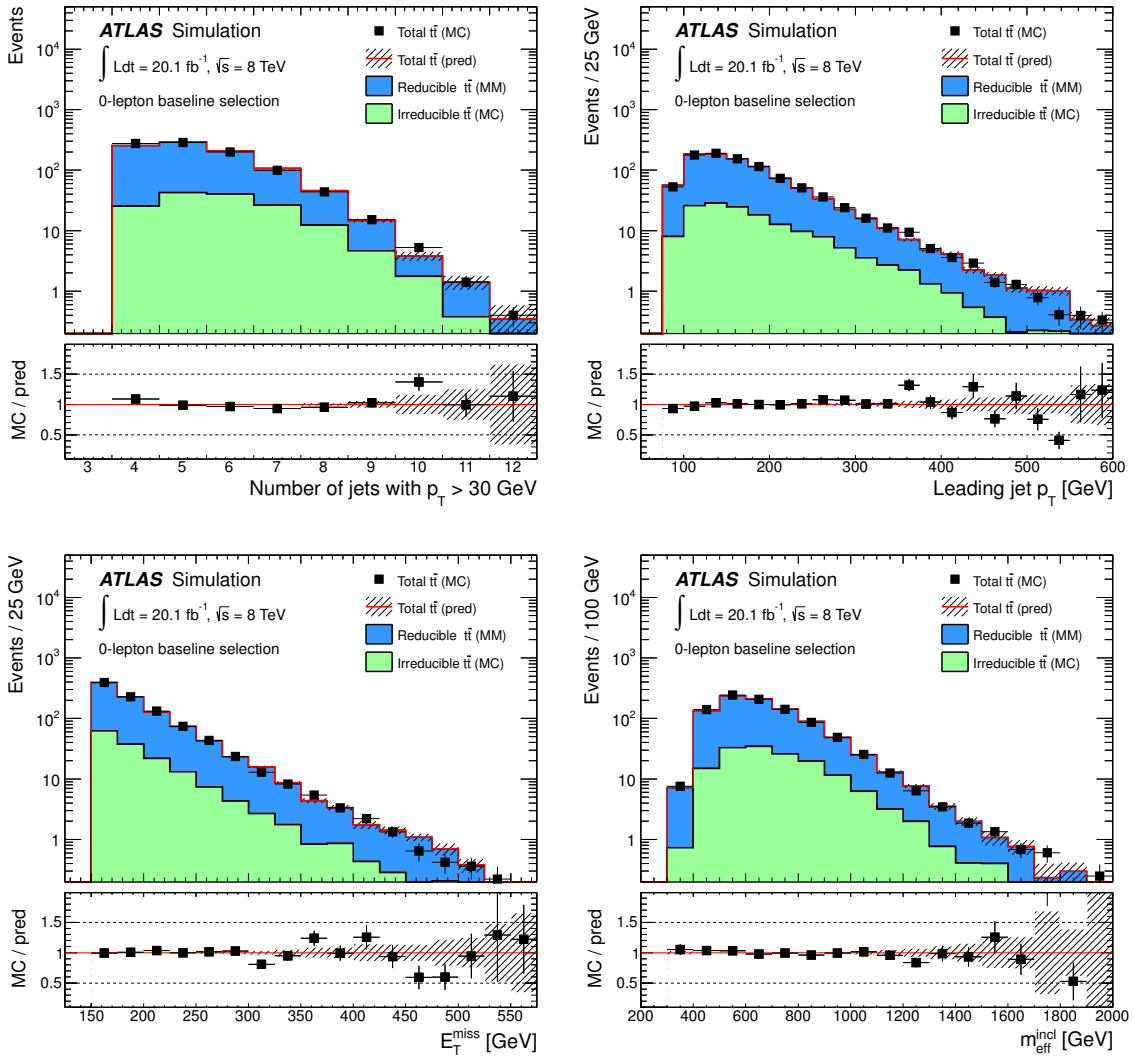

Figure 1: Closure test of the matrix method used to determine the reducible background contribution. The number of jets with $p_{\mathrm{T}} > 30$ GeV, the leading jet p_{T}, the $E_{\mathrm{T}}^{\mathrm{miss}}$ and the $m_{\mathrm{eff}}^{\mathrm{incl}}$ distributions as predicted by the matrix method applied on MC in the 0-lepton channel. The prediction from the matrix method (MM) applied on MC is shown in dark gray (blue), the irreducible $t\bar{t}$ + $b/b\bar{b}$ component from MC is shown in light gray (green) and the total $t\bar{t}$ MC prediction is shown with the black points. The ratio between the event yield in pure MC prediction and the matrix method prediction is also shown. Only the statistical uncertainties on the MC predictions are shown.

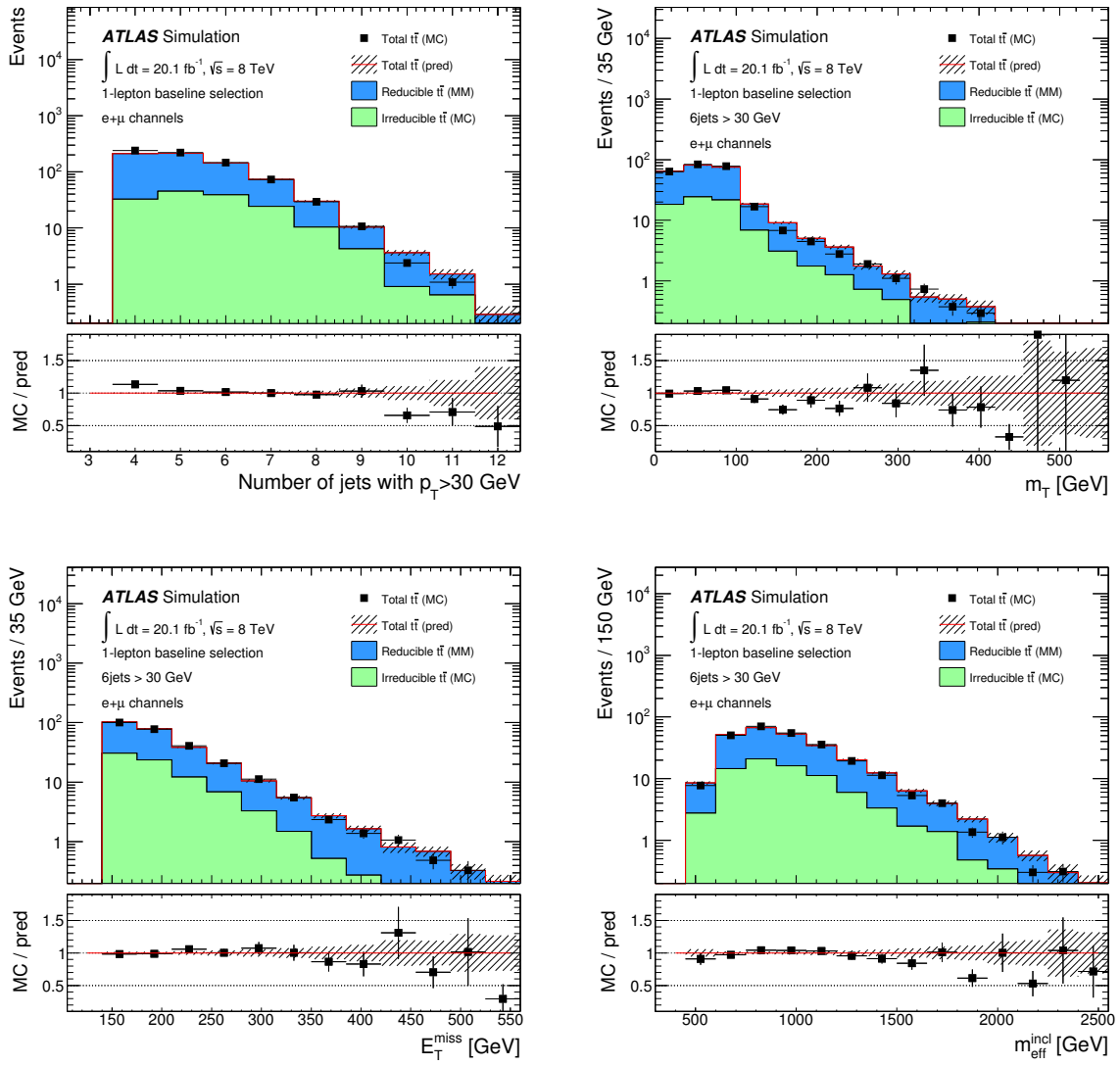

Figure 2: Closure test of the matrix method used to determine the reducible background contribution. The distribution of the number of jets with $p_{\mathrm{T}} > 30$ GeV for events with at least 4 jets, and the m_{T}, the $E_{\mathrm{T}}^{\mathrm{miss}}$ and the $m_{\mathrm{eff}}^{\mathrm{incl}}$ distributions for events with at least 6 jets, as predicted by the matrix method applied on MC in the 1-lepton channel. The prediction from the matrix method (MM) applied on MC is shown in dark gray (blue), the irreducible $t\bar{t} + b/b\bar{b}$ component from MC is shown in light gray (green) and the total $t\bar{t}$ MC prediction is shown with the black points. The ratio between the event yield in pure MC prediction and the matrix method prediction is also shown. Only the statistical uncertainties on the MC predictions are shown.

of 1 GeV of the top quark mass. Finally, systematic uncertainties in the modelling of the $t\bar{t}+b/b\bar{b}$ background are also considered, that are assessed as follows: the uncertainties due to the choice of the factorisation (μ_F) and renormalisation (μ_R) scales in POWHEG are estimated by comparing the baseline sample to POWHEG+Pythia samples generated with μ_F and μ_R varied separately up and down by a factor of two or half. The MC generator uncertainty is estimated by comparing POWHEG with the PDF set CT10 to the leading-order ALPGEN generator [68] with the PDF set CTEQ6L1, both interfaced to HERWIG and JIMMY; the parton shower uncertainty is assessed by comparing POWHEG interfaced to PYTHIA6 to POWHEG interfaced to HERWIG and JIMMY, both with the PDF set CT10; the uncertainty due the initial (ISR) and final (FSR) state radiation is estimated by comparing AcerMC MC samples interfaced to PYTHIA6, using the PDF set CTEQ6L1 and generated with modified ISF/FSR modelling. The variation of the ISR/FSR parameters has been validated with data in an analysis of rapidity gaps between jets in $t\bar{t}$ events [69]. For the $t\bar{t}+Z/h$ backgrounds, a 100% uncertainty is used.

A systematic uncertainty in the matrix method prediction of the reducible backgrounds arises from the uncertainties in the measurement of the b-tagging efficiency and mistag rate. The difference between the baseline prediction obtained with the mistag rate estimated in $t\bar{t}$ MC and the prediction obtained using the mistag rate measured in data is assigned as systematic uncertainty. The statistical uncertainties in these two mistag rates due to the limited statistics in data and in the $t\bar{t}$ MC sample are also taken into account. The uncertainties on the modelling of the b-tagging efficiencies in the simulation, measured separately for the different jets flavours, are included in the uncertainties on the mistag rate extracted from MC and are treated as fully correlated with the corresponding uncertainties on the irreducible background and the signal. The statistical uncertainty on the number of observed events for each b-jet multiplicity is propagated to the matrix method prediction. The latter uncertainty is the dominant source of uncertainty on the background estimation in the signal regions.

Finally, an uncertainty on the integrated luminosity of $\pm$ 2.8% is also considered. It is derived, following the same methodology as that detailed in Ref. [70], from a preliminary calibration of the luminosity scale derived from beam-separation scans performed in November 2012.

9 Results

Figure 3 shows on the left (right) the number of jets with $p_{\mathrm{T}} > 30$ (50) GeV distributions observed in data after the 0-lepton baseline selection and after requiring at least 4 jets with $p_{\mathrm{T}} > 30$ (50) GeV, together with the background prediction from the matrix method for the reducible background and from MC for the irreducible background. The $E_{\mathrm{T}}^{\mathrm{miss}}$ and $m_{\mathrm{eff}}^{\mathrm{4j}}$ distributions after requiring at least 4 jets with $p_{\mathrm{T}} > 30$ GeV and 4 jets with $p_{\mathrm{T}} > 50$ GeV are shown on Figures 4 and 5, respectively. The $E_{\mathrm{T}}^{\mathrm{miss}}$ and $m_{\mathrm{eff}}^{\mathrm{incl}}$ for events with 7 jets with $p_{\mathrm{T}} > 30$ GeV are shown on Figure 6. Figure 7 shows the m_{T} distribution after the 1-lepton baseline selection, and the distribution of the number of jets with $p_{\mathrm{T}} > 30$ GeV, the $E_{\mathrm{T}}^{\mathrm{miss}}$ and $m_{\mathrm{eff}}^{\mathrm{incl}}$ observed in data after an additional requirement of $m_{\mathrm{T}} > 100$ GeV. Also shown are the predictions of two benchmark signal models. The SM predictions agree with the data within the uncertainties for all distributions. The background predictions obtained with the matrix method in all validation regions, compared with the observed number of events in data, are shown in Table 3. The expected background yields as predicted from MC simulations only are also shown in parentheses. An overall good agreement within the uncertainties is observed between the predicted and observed event yields in all validation regions. The results in the signal regions are shown in Table 4. The number of events observed in the signal regions of the 0-lepton channel are con-

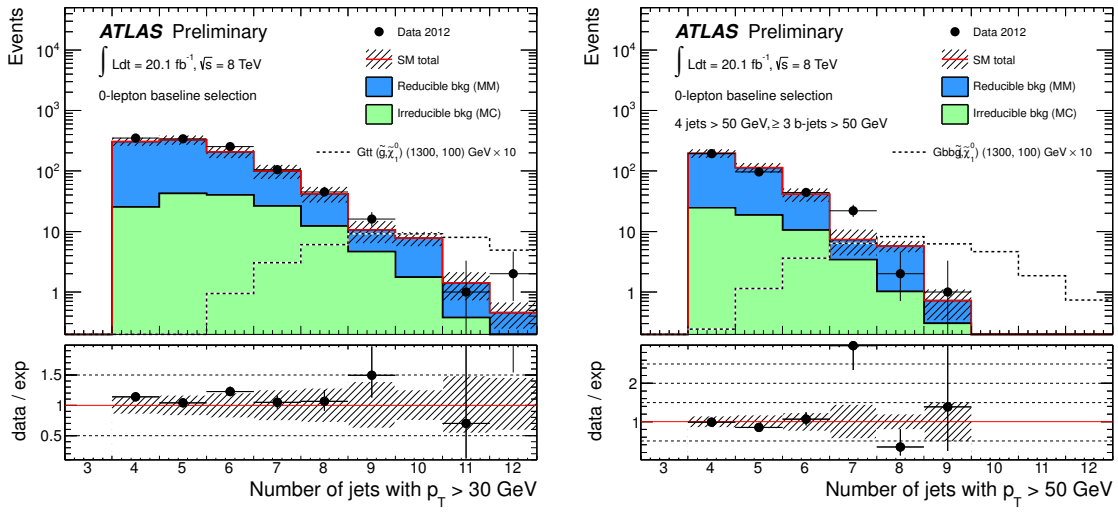

Figure 3: *Left (right):* The number of jets with $p_{\mathrm{T}} > 30$ (50) GeV observed in data after the 0-lepton baseline selection and after requiring at least 4 jets with $p_{\mathrm{T}} > 30$ (50) GeV, together with the background prediction. The prediction from the matrix method for the reducible background (MM) is shown in dark gray (blue) and the irreducible background from MC is shown in light gray (green). The predictions for two signal points from the *Gbb* ($\tilde{g} \to b\bar{b}\tilde{\chi}_1^0$) and *Gtt* ($\tilde{g} \to t\bar{t}\tilde{\chi}_1^0$) models are overlaid. The ratio between the observed event yield and background prediction is also shown. The shaded bands include all systematic uncertainties on the MC and the matrix method predictions.

sistent with the SM expectations. In the 1-lepton channel, a deficit in data corresponding to a background fluctuation probability of around 15% in SR-1l-6j-A is observed. Since they are correlated, the effect is observed in all 1-lepton signal regions, and can be already observed in the 6th jet bin in Figure 7. However the observed event yield is still consistent with the SM prediction given the large uncertainties on the background prediction.

10 Interpretations

The results of this analysis are used to derive upper limits on the number of non-SM signal events in each signal region, and model-dependent exclusion limits in the context of several SUSY models described in Section 2. All limits are calculated at 95% CL by testing the signal plus background hypothesis using the profile likelihood method with the CL_s prescription [71]. The limits on new physics are derived with pseudo-experiments, while the model-dependent exclusion limits are calculated with the asymptotic formulae [72].

10.1 Limits on new physics

Upper limits on the number of signal events and on the visible cross-section for non-SM contributions in each signal region, defined in terms of the kinematic acceptance A and the experimental efficiency ε as $\sigma_{vis} = \sigma \times A \times \varepsilon$, are given in Table 5. These limits are derived with pseudo-experiments, and the results obtained with the asymptotic formulae are given in parentheses for comparison. The systematic uncertainties on the SM background estimation discussed in Section 8 are included, but no systematic uncertainties are assumed for the signal.

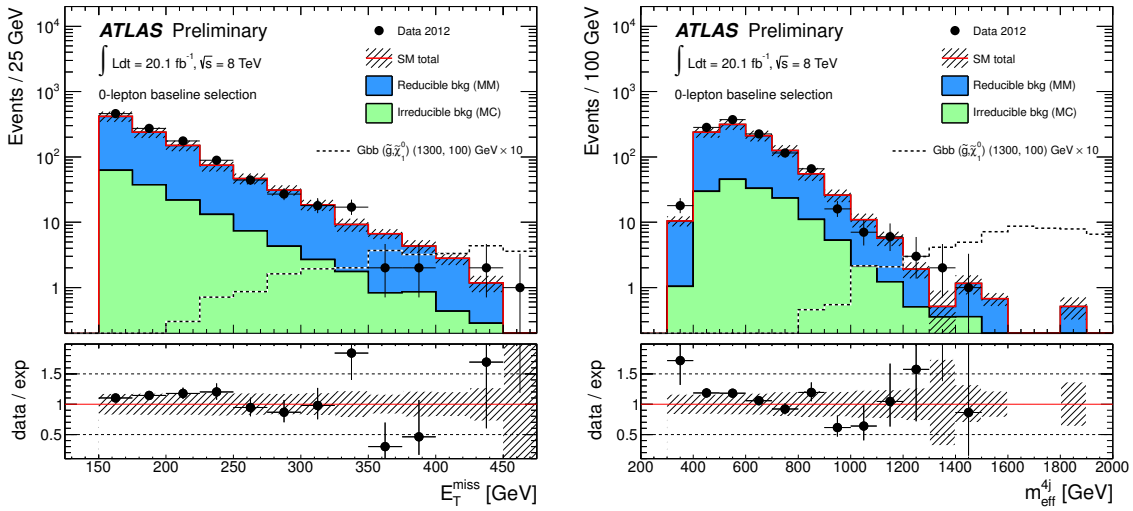

Figure 4: The $E_{\mathrm{T}}^{\mathrm{miss}}$ and $m_{\mathrm{eff}}^{\mathrm{4j}}$ distributions observed in data together with the background prediction from the matrix method for the reducible background and from the MC for the irreducible background in the 0-lepton channel after requiring at least 4 jets with $p_{\mathrm{T}} > 30$ GeV. The prediction from the matrix method for the reducible background (MM) is shown in dark gray (blue) and the irreducible background from MC is shown in light gray (green). The prediction for one signal point from the *Gbb* ($\tilde{g} \to b\bar{b}\tilde{\chi}_1^0$) model is overlaid. The ratio between the observed event yield and background prediction is also shown. The shaded bands include all systematic uncertainties on the MC and the matrix method predictions.

region	reducible bkg	irreducible bkg	total bkg (MC)	data
VR-0l-4j-A	840 ± 120	150 ± 120	990 ± 170 (1020)	1101
VR-0l-4j-B	300 ± 50	60 ± 50	360 ± 70 (360)	360
VR-0l-7j-A	97 ± 16	36 ± 32	130 ± 40 (140)	140
VR-0l-7j-B	115 ± 22	40 ± 40	160 ± 40 (170)	165
VR-1l-4j	41 ± 18	18 ± 14	59 ± 23 (64)	75
VR-1l-6j	16 ± 10	9.3 ± 7.1	25 ± 12 (24)	17

Table 3: Background predictions obtained in all validation regions compared with the observed number of events in data. The reducible background is estimated with the matrix method while the irreducible background is extracted from MC simulations. All systematic uncertainties are included. The total background as predicted from MC simulations only is shown in parentheses.

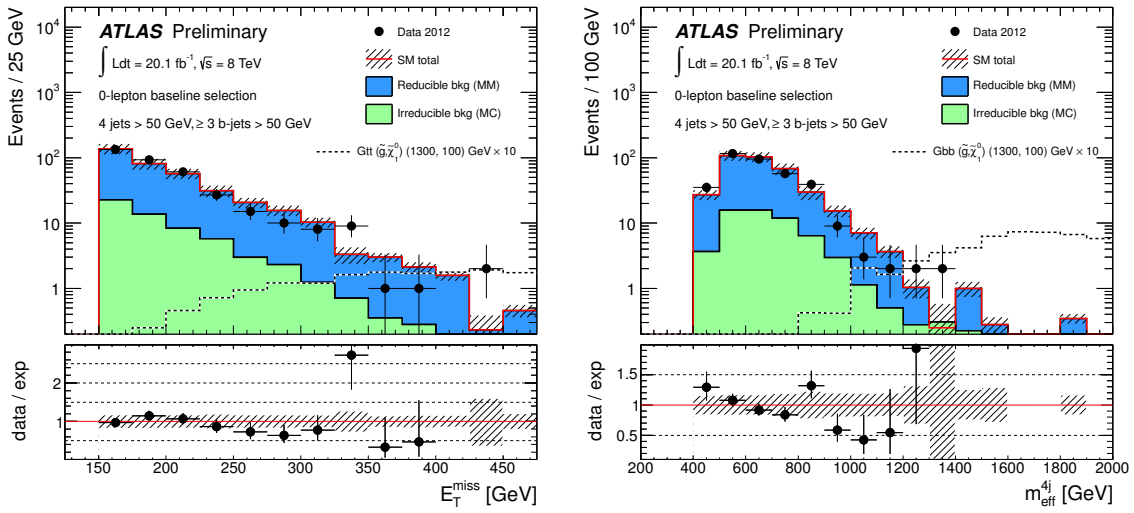

Figure 5: The $E_{\mathrm{T}}^{\mathrm{miss}}$ and $m_{\mathrm{eff}}^{\mathrm{4j}}$ distributions observed in data together with the background prediction from the matrix method for the reducible background and from the MC for the irreducible background in the 0-lepton channel after requiring at least 4 jets with $p_{\mathrm{T}} > 50$ GeV. The prediction from the matrix method for the reducible background (MM) is shown in dark gray (blue) and the irreducible background from MC is shown in light gray (green). The prediction for one signal point from the *Gbb* ($\tilde{g} \to b\bar{b}\tilde{\chi}_1^0$) model is overlaid. The ratio between the observed event yield and background prediction is also shown. The shaded bands include all systematic uncertainties on the MC and the matrix method predictions.

region	reducible bkg	irreducible bkg	total bkg (MC)	data
SR-0l-4j-A	2.2 ± 1.1	0.8 ± 0.7	3.0 ± 1.3 (5.1)	2
SR-0l-4j-B	0.8 ± 0.9	0.5 ± 0.5	1.3 ± 1.0 (3.9)	3
SR-0l-4j-C	1.2 ± 0.8	0.6 ± 0.6	1.8 ± 1.0 (2.5)	2
SR-0l-7j-A	15.5 ± 3.4	7.0 ± 6.0	22.5 ± 6.9 (28.8)	22
SR-0l-7j-B	2.3 ± 2.3	1.3 ± 1.1	3.6 ± 2.5 (6.2)	3
SR-0l-7j-C	$0 \pm 0.5^{+0.5}_{-0}$	0.8 ± 0.7	$0.8 \pm {}^{+0.9}_{-0.8}$ (3.1)	1
SR-1l-6j-A	$10.7\ {}^{+7.5}_{-6.8}$	4.8 ± 3.7	15.5 ± 8.4 (13.8)	7
SR-1l-6j-B	5.7 ± 5.5	1.7 ± 1.4	7.4 ± 5.7 (6.3)	0
SR-1l-6j-C	$2.4\ {}^{+2.7}_{-2.4}$	$0.6\ {}^{+0.6}_{-0.5}$	3.0 ± 2.8 (2.6)	0

Table 4: Background predictions obtained in all signal regions compared with the observed number of events in data. The reducible background is estimated with the matrix method while the irreducible background is extracted from MC simulations. All systematic uncertainties are included. The total background as predicted from MC simulations only is shown in parentheses.

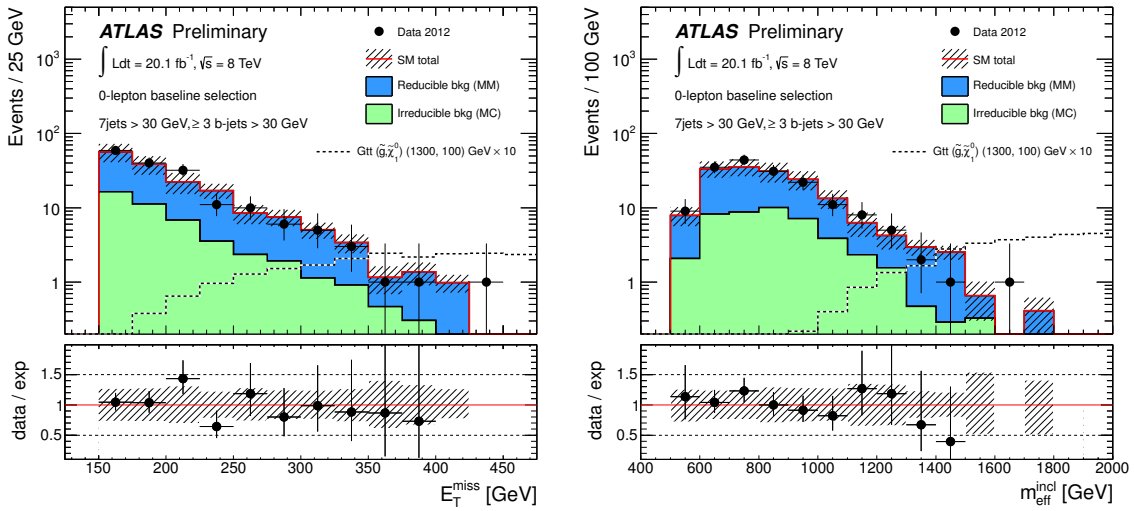

Figure 6: The $E_{\mathrm{T}}^{\mathrm{miss}}$ and $m_{\mathrm{eff}}^{\mathrm{incl}}$ distributions observed in data together with the background prediction from the matrix method for the reducible background and from the MC for the irreducible background in the 0-lepton channel after requiring at least 7 jets with $p_{\mathrm{T}} > 30$ GeV. The prediction from the matrix method for the reducible background (MM) is shown in dark gray (blue) and the irreducible background from MC is shown in light gray (green). The prediction for one signal point from the Gtt ($\tilde{g} \to t\bar{t}\tilde{\chi}_1^0$) model is overlaid. The ratio between the observed event yield and background prediction is also shown. The shaded bands include all systematic uncertainties on the MC and the matrix method predictions.

SR	95% CL UL on N_{BSM}		95% CL UL on $\sigma \times A \times \varepsilon$ [fb]	
	Observed	Expected	Observed	Expected
SR-0l-4j-A	4.6 (4.3)	$5.0^{+2.0}_{-1.3}$ (5.0)	0.23	0.25
SR-0l-4j-B	6.7 (6.2)	$5.0^{+1.5}_{-0.8}$ (4.5)	0.33	0.25
SR-0l-4j-C	4.8 (4.6)	$4.4^{+1.7}_{-1.0}$ (4.4)	0.24	0.22
SR-0l-7j-A	15.3 (14.4)	$14.6^{+6.1}_{-3.4}$ (14.6)	0.76	0.73
SR-0l-7j-B	6.1 (5.7)	$6.0^{+2.3}_{-1.0}$(6.0)	0.30	0.30
SR-0l-7j-C	3.9 (3.6)	$3.6^{+1.2}_{-0.5}$ (3.5)	0.19	0.18
SR-1l-6j-A	6.6 (6.9)	$9.5^{+3.9}_{-2.9}$ (9.5)	0.33	0.47
SR-1l-6j-B	3.0 (2.6)	$3.9^{+1.7}_{-1.0}$ (4.4)	0.15	0.19
SR-1l-6j-C	3.0 (2.3)	$3.1^{+0.9}_{-0.0}$ (3.1)	0.15	0.15

Table 5: Observed and expected new-physics upper limits (UL) at 95% CL for all signal regions. Limits are given on the number of signal events N_{BSM} and in terms of visible cross-section defined as $\sigma_{vis} = \sigma \times A \times \varepsilon$. The limits are derived with pseudo-experiments, and the results obtained with the asymptotic formulae are given in parentheses for comparison. The systematic uncertainties on the SM background estimation discussed in Section 8 are included.

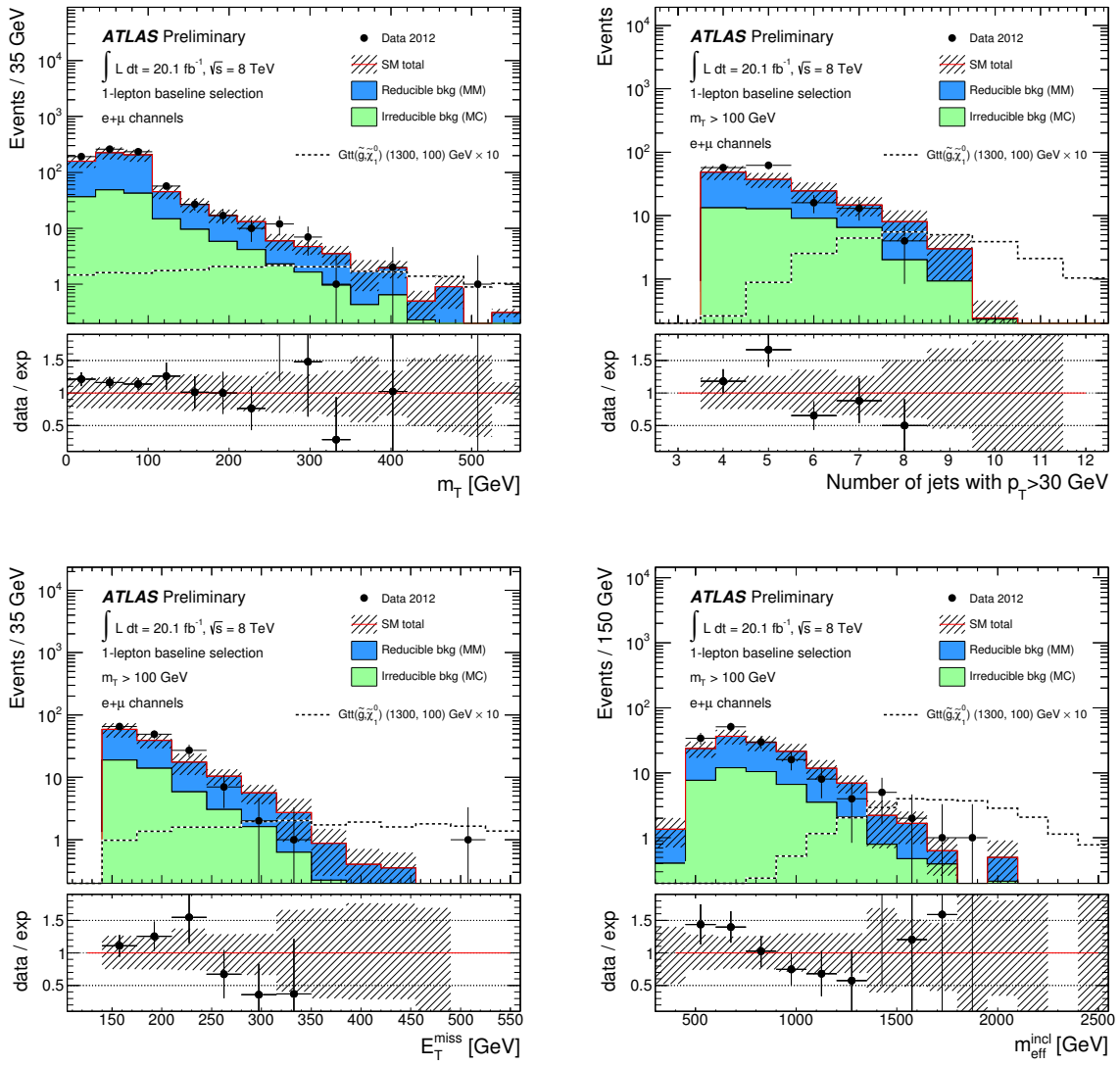

Figure 7: The m_{T} distribution for the baseline selection in the 1-lepton channel, and the number of jets with $p_{\mathrm{T}} > 30$ GeV, the $E_{\mathrm{T}}^{\mathrm{miss}}$ and the $m_{\mathrm{eff}}^{\mathrm{incl}}$ distributions after requiring $m_{\mathrm{T}} > 100$ GeV, as observed in data together with the background prediction from the matrix method for the reducible background (MM) and from the MC for the irreducible background. The prediction from the matrix method for the reducible background is shown in dark gray (blue) and the irreducible background from MC is shown in light gray (green). The prediction for one signal point from the Gtt ($\tilde{g} \to t\bar{t}\tilde{\chi}_1^0$) model is overlaid. The ratio between the observed event yield and background prediction is also shown. The shaded bands include all systematic uncertainties on the MC and the matrix method predictions.

10.2 Model-dependent exclusion limits

The results are used to derive exclusion limits in the context of the SUSY models described in Section 2. The SR-0l-4j signal regions are mostly sensitive to the gluino decays $\tilde{g} \to b\bar{b}\tilde{\chi}_1^0$ via on-shell or off-shell sbottom, whilst the SR-0l-7j and SR-1l signal regions are used to set exclusion limits in models where top-enriched final states are expected. The 0-lepton and 1-lepton channels are also combined for the direct sbottom scenario, where a Higgs boson can decay producing leptons in the final state.

Limits are derived using the signal region yielding the best expected sensitivity for each point in the parameter space, before unblinding the data in the signal regions. For signal models where both the 0- and 1-lepton channels contribute to the sensitivity, they are combined in a simultaneous fit to enhance the sensitivity of the analysis. In this case, all possible permutations between the three 1-lepton and the six 0-lepton signal regions are considered in each point of the parameter space and the best expected combination is used.

The experimental systematic uncertainties are treated as fully correlated between the signal and the SM background and between the 0- and 1-lepton channels. They are dominated by the JES and b-tagging uncertainties, which typically amount to 2–25% depending on the signal region and model considered. The theoretical uncertainties on the irreducible background component are also treated as fully correlated between the two channels.

Theoretical uncertainties on the SUSY signals are estimated as described in Section 4. Limits are calculated for the nominal cross-section, and for the $\pm 1\sigma^{\text{SUSY}}_{\text{Theory}}$ cross-sections. All limits quoted in the text correspond to the $-1\sigma^{\text{SUSY}}_{\text{Theory}}$ hypothesis.

The expected and observed exclusion limits resulting from the combination of the 0-lepton and the 1-lepton channels for the direct sbottom scenario are shown in Figure 8. Sbottom masses between 320 and 600 GeV are excluded for $m_{\tilde{\chi}_2^0} = 300$ GeV. No exclusion limits are obtained for low $m_{\tilde{\chi}_2^0}$ due to the presence of soft b-jets in the final states. The sensitivity of this analysis to $\tilde{b}_1$ pair production processes where $\tilde{b}_1 \to b + \tilde{\chi}_2^0$, $\tilde{\chi}_2^0 \to h + \tilde{\chi}_1^0$, depends on $m_{\tilde{\chi}_1^0}$. For higher neutralino masses, the sensitivity decreases because of the tight $E_{\text{T}}^{\text{miss}}$ and the jets p_{T} thresholds.

The expected and observed exclusion limits for the Gluino-Sbottom and Gluino-Stop scenarios are shown in Figure 9. In the Gluino-Sbottom model, gluino masses below 1200 GeV are excluded for sbottom masses up to about 1000 GeV. This extends by approximately 200 GeV the limits derived in the same scenario by the previous analysis performed with 4.7 fb^{-1} at $\sqrt{s}$ = 7 TeV [22] and is complementary to the ATLAS search for direct sbottom pair production, also carried out with the full data set collected by ATLAS at $\sqrt{s}$ = 8 TeV [73]. The exclusion is less stringent in the region with low $m_{\tilde{g}} - m_{\tilde{b}_1}$, where softer jets are expected.

In the Gluino-Stop models, a combination of both 0- and 1-lepton channels is used to derive the limit contours. For the Gluino-Stop I model, gluino masses below 1050 GeV are excluded for stop masses up to 850 GeV, significantly extending the previous ATLAS limits [22], while for the Gluino-Stop II model gluino masses below 1320 GeV are excluded for stop masses up to 1150 GeV. The sensitivity is lower in the Gluino-Stop I model where soft $E_{\text{T}}^{\text{miss}}$ and jets are expected from the chargino decay into the neutralino plus a virtual W boson. These limits are complementary to the ATLAS searches for direct stop pair production performed in the 0-lepton [74] and 1-lepton [75] channels with the full data set collected by ATLAS at $\sqrt{s}$ = 8 TeV.

The expected and observed exclusion limits in the $(m_{\tilde{g}}, m_{\tilde{\chi}_1^0})$ plane for the Gbb, Gtt and Gtb models are shown in Figure 10. In the context of the Gbb model, gluino masses below 1200 GeV are excluded for $m_{\tilde{\chi}_1^0} < 600$ GeV. Lower sensitivity is achieved at very low mass splitting between the gluino and the neutralino because of the presence of soft b-jets and low $E_{\text{T}}^{\text{miss}}$ expected

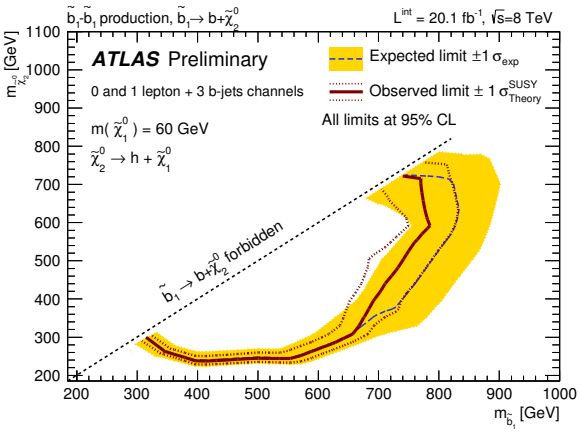

Figure 8: Exclusion limits in the $(m_{\tilde{b}_1}, m_{\tilde{\chi}_2^0})$ plane for the Direct-Sbottom model. The dashed blue and solid bold red lines show the 95% CL expected and observed limits respectively, including all uncertainties except the theoretical signal cross-section uncertainty. The shaded (yellow) bands around the expected limits show the impact of the experimental and background theoretical uncertainties while the dotted red lines show the impact on the observed limit of the variation of the nominal signal cross-section by 1σ of its theoretical uncertainty.

in signal events. The improvement in this region with respect to the previous analysis carried out with 12.8 fb^{-1} [21] is due to the use of signal MC samples generated with MADGRAPH which ensures an accurate treatment of the recoil against an ISR jet. The uncertainty on the ISR modeling, assessed by comparing the signal event yield predicted by MADGRAPH and Herwig++, is parameterised as a function of the mass splitting and is included in the experimental uncertainty band. In the context of the Gtt model, gluino masses below 1340 GeV are excluded for $m_{\tilde{\chi}_1^0} < 400$ GeV while neutralino masses below 620 GeV are excluded for $m_{\tilde{g}} = 1000$ GeV. The SR-0l-7j signal regions have the best sensitivity at large mass splitting between the gluino and the neutralino, where hard jets and $E_{\mathrm{T}}^{\mathrm{miss}}$ are expected, while the SR-1l signal regions have a better sensitivity close to the kinematic boundary. In the context of the Gtb model, gluino masses below 1300 GeV are excluded for $m_{\tilde{\chi}_1^0} < 300$ GeV while neutralino masses below 580 GeV are excluded for $m_{\tilde{g}} = 1100$ GeV.

The expected and observed exclusion limits in the $(m_0, m_{\frac{1}{2}})$ plane of the mSUGRA/CMSSM model are shown in Figure 11. For universal scalar masses m_0 up to 6 TeV, gluino masses smaller than 1280 GeV are excluded. This analysis is especially sensitive to the high m_0 region where four top quarks final states dominate.

11 Conclusions

In summary, this note presents results of a search for gluino and sbottom pair production with multi-b-jets final states in pp collisions at $\sqrt{s}$ = 8 TeV, based on 20.1 fb^{-1} of ATLAS data. The events are selected with large $E_{\mathrm{T}}^{\mathrm{miss}}$, several jets and at least three jets tagged as originating from b-quarks in the final state. The analysis is carried out in the orthogonal 0- and 1- lepton channels which are combined to improve the sensitivity to physics beyond the Standard Model processes. The results are in agreement with the SM background predictions and translate into 95% CL upper limits on excluded masses for several SUSY scenarios. Gluino masses up to about 1.3 TeV are excluded, depending on the model, which significantly extends previous

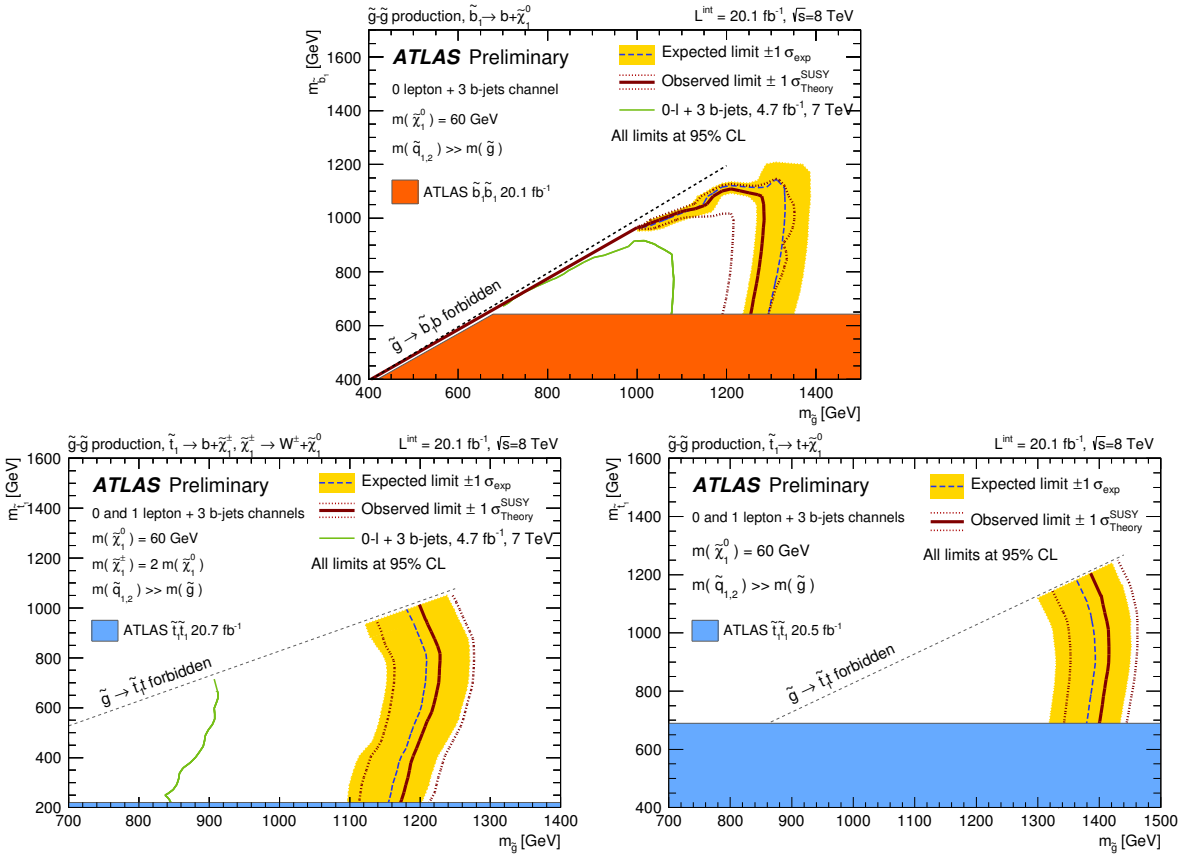

Figure 9: *Top:* Exclusion limits in the $(m_{\tilde{g}}, m_{\tilde{b}_1})$ plane for the Gluino-Sbottom model. *Bottom:* Exclusion limits in the $(m_{\tilde{g}}, m_{\tilde{t}_1})$ plane for the Gluino-Stop I *(left)* and II *(right)* models. The dashed blue and solid bold red lines show the 95% CL expected and observed limits respectively, including all uncertainties except the theoretical signal cross-section uncertainty. The shaded (yellow) bands around the expected limits show the impact of the experimental and background theoretical uncertainties while the dotted red lines show the impact on the observed limit of the variation of the nominal signal cross-section by 1σ of its theoretical uncertainty. Also shown for reference are the results from previous ATLAS analyses [22, 73–75] derived using the nominal cross section.

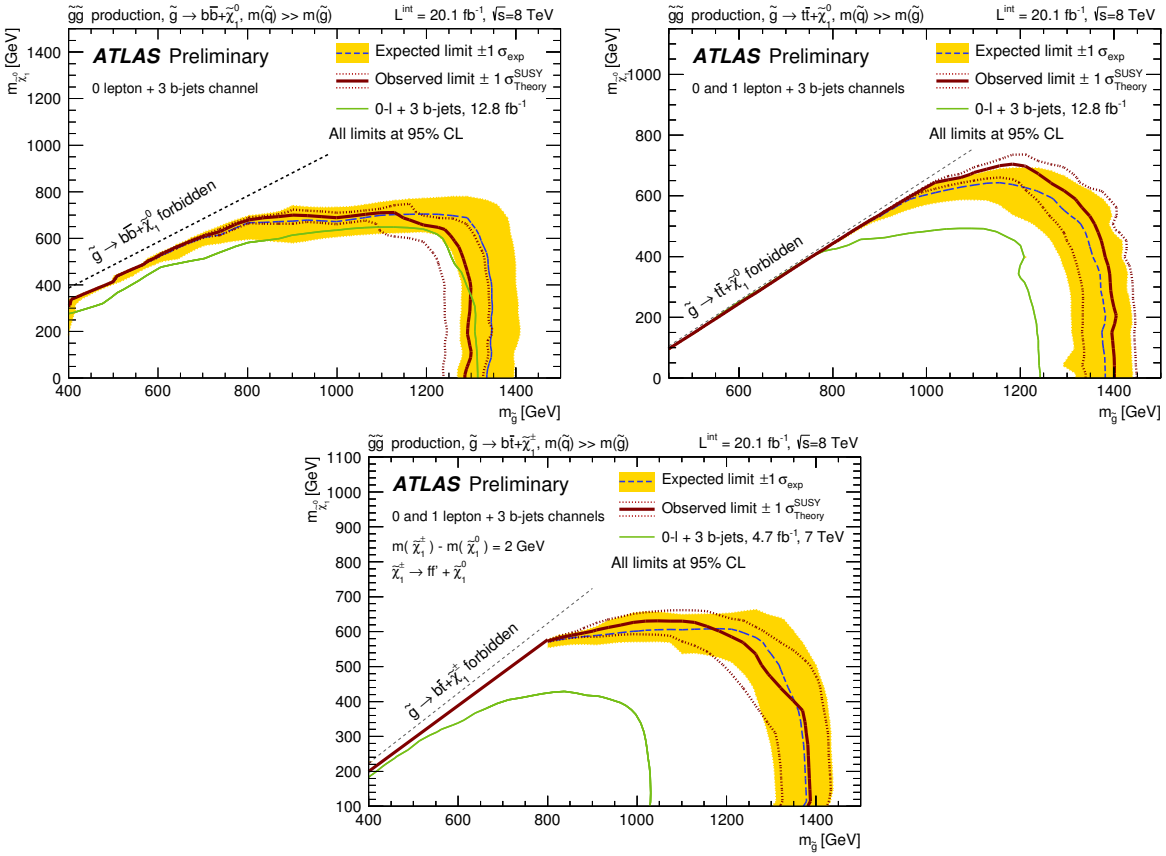

Figure 10: Exclusion limits in the $(m_{\tilde{g}}, m_{\tilde{\chi}_1^0})$ plane for the Gbb (top left), Gtt (top right) and Gtb (bottom) models. The dashed blue and solid bold red lines show the 95% CL expected and observed limits respectively, including all uncertainties except the theoretical signal cross-section uncertainty. The shaded (yellow) bands around the expected limits show the impact of the experimental and background theoretical uncertainties while the dotted red lines show the impact on the observed limit of the variation of the nominal signal cross-section by 1σ of its theoretical uncertainty. Also shown for reference are the results from previous ATLAS analyses [21,22] derived using the nominal cross section.

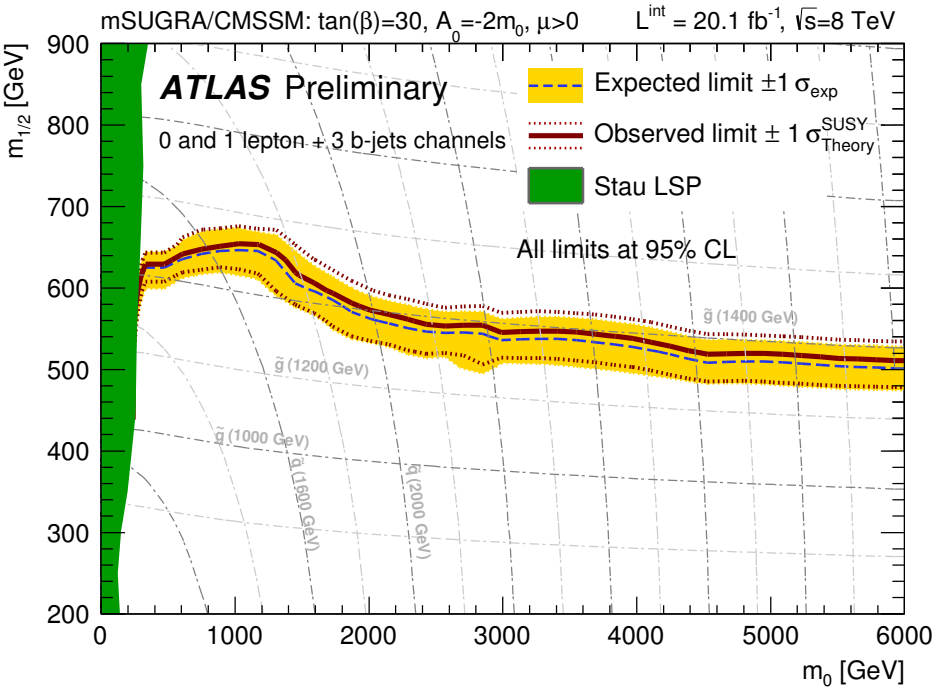

Figure 11: Exclusion limits in the $(m_0, m_{\frac{1}{2}})$ plane for the mSUGRA/CMSSM model. The dashed blue and solid bold red lines show the 95% CL expected and observed limits respectively, including all uncertainties except the theoretical signal cross-section uncertainty. The shaded (yellow) bands around the expected limits show the impact of the experimental and background theoretical uncertainties while the dotted red lines show the impact on the observed limit of the variation of the nominal signal cross-section by 1σ of its theoretical uncertainty.

ATLAS results.

References

[1] H. Miyazawa, *Baryon Number Changing Currents*, Prog. Theor. Phys. **36 (6)** (1966) 1266–1276.

[2] P. Ramond, *Dual Theory for Free Fermions*, Phys. Rev. D **3** (1971) 2415–2418.

[3] Y. Golfand and E. Likhtman, *Extension of the Algebra of Poincare Group Generators and Violation of p Invariance*, JETP Lett. **13** (1971) 323–326.

[4] A. Neveu and J. H. Schwarz, *Factorizable dual model of pions*, Nucl. Phys. B **31** (1971) 86–112.

[5] A. Neveu and J. H. Schwarz, *Quark Model of Dual Pions*, Phys. Rev. D **4** (1971) 1109–1111.

[6] J. Gervais and B. Sakita, *Field theory interpretation of supergauges in dual models*, Nucl. Phys. B **34** (1971) 632–639.

[7] D. Volkov and V. Akulov, *Is the Neutrino a Goldstone Particle?*, Phys. Lett. B **46** (1973) 109–110.

[8] J. Wess and B. Zumino, *A Lagrangian Model Invariant Under Supergauge Transformations*, Phys. Lett. B **49** (1974) 52.

[9] J. Wess and B. Zumino, *Supergauge Transformations in Four-Dimensions*, Nucl. Phys. B **70** (1974) 39–50.

[10] S. Weinberg, *Implications of Dynamical Symmetry Breaking*, Phys. Rev. D **13** (1976) 974–996.

[11] E. Gildener, *Gauge Symmetry Hierarchies*, Phys. Rev. D **14** (1976) 1667.

[12] S. Weinberg, *Implications of Dynamical Symmetry Breaking: An Addendum*, Phys. Rev. D **19** (1979) 1277–1280.

[13] L. Susskind, *Dynamics of Spontaneous Symmetry Breaking in the Weinberg- Salam Theory*, Phys. Rev. D **20** (1979) 2619–2625.

[14] P. Fayet, *Supersymmetry and Weak, Electromagnetic and Strong Interactions*, Phys. Lett. B **64** (1976) 159.

[15] P. Fayet, *Spontaneously Broken Supersymmetric Theories of Weak, Electromagnetic and Strong Interactions*, Phys. Lett. B **69** (1977) 489.

[16] G. R. Farrar and P. Fayet, *Phenomenology of the Production, Decay, and Detection of New Hadronic States Associated with Supersymmetry*, Phys. Lett. B **76** (1978) 575–579.

[17] P. Fayet, *Relations Between the Masses of the Superpartners of Leptons and Quarks, the Goldstino Couplings and the Neutral Currents*, Phys. Lett. B **84** (1979) 416.

[18] S. Dimopoulos and H. Georgi, *Softly Broken Supersymmetry and SU(5)*, Nucl. Phys. B **193** (1981) 150.

[19] R. Barbieri and G. Giudice, *Upper Bounds on Supersymmetric Particle Masses*, Nucl.Phys. **B306** (1988) 63.

[20] B. de Carlos and J. Casas, *One loop analysis of the electroweak breaking in supersymmetric models and the fine tuning problem*, Phys.Lett. **B309** (1993) 320–328, arXiv:hep-ph/9303291 [hep-ph].

[21] ATLAS Collaboration, *Search for gluino pair production in final states with missing transverse momentum and at least three b-jets using 12.8 fb^{-1} of pp collisions at $\sqrt{s}$ = 8 TeV with the ATLAS detector*, ATLAS-CONF-2012-145 (2012). http://cdsweb.cern.ch/record/1493484.

[22] ATLAS Collaboration, *Search for top and bottom squarks from gluino pair production in final states with missing transverse energy and at least three b-jets with the ATLAS detector*, Eur.Phys.J.C **72** (2012) 2174, arXiv:1207.4686 [hep-ex].

[23] ATLAS Collaboration, *Search for strongly produced superpartners in final states with two same sign leptons with the ATLAS detector using 21 fb^{-1} of proton-proton collisions at $\sqrt{s}$ = 8 TeV*, ATLAS-CONF-2013-007 (2013). http://cdsweb.cern.ch/record/1522430.

[24] ATLAS Collaboration, *Search for new phenomena using final states with large jet multiplicities and missing transverse momentum with ATLAS in 20 fb^{1} of $\sqrt{s}$ = 8 TeV proton-proton collisions*, ATLAS-CONF-2013-054 (2013). http://cdsweb.cern.ch/record/1547571.

[25] ATLAS Collaboration, *Search for squarks and gluinos with the ATLAS detector in final states with jets and missing transverse momentum and 20.3 fb^{1} of $\sqrt{s}$ = 8 TeV proton-proton collision data*, ATLAS-CONF-2013-047 (2013). http://cdsweb.cern.ch/record/1547563.

[26] CMS Collaboration, *Search for Supersymmetry in pp collisions at 8 TeV in events with a single lepton, multiple jets and b-tags*, CMS-PAS-SUS-13-007 (2013). http://cdsweb.cern.ch/record/1523786.

[27] CMS Collaboration, *Search for supersymmetry in the 3 lepton + b-tag final state in pp collisions at 8 TeV*, CMS-PAS-SUS-13-008 (2013). http://cdsweb.cern.ch/record/1547560.

[28] ATLAS Collaboration, *The ATLAS Experiment at the CERN Large Hadron Collider*, JINST **3** (2008) S08003.

[29] S. Frixione, P. Nason, and C. Oleari, *Matching NLO QCD computations with Parton Shower simulations: the POWHEG method*, J. High Energy Phys. **0711** (2007) 070, arXiv:0709.2092 [hep-ph].

[30] T. Sjöstrand, S. Mrenna, and P. Z. Skands, *PYTHIA 6.4 Physics and Manual*, J. High Energy Phys. **0605** (2006) 026, arXiv:hep-ph/0603175 [hep-ph].

[31] P. Z. Skands, *Tuning Monte Carlo Generators: The Perugia Tunes*, Phys.Rev. **D82** (2010) 074018, arXiv:1005.3457 [hep-ph].

[32] H.-L. Lai et al., *New parton distributions for collider physics*, Phys. Rev. D **82** (2010) 074024, arXiv:1007.2241 [hep-ph].

[33] B. P. Kersevan and E. Richter-Was, *The Monte Carlo event generator AcerMC version 2.0 with interfaces to PYTHIA 6.2 and HERWIG 6.5*, arXiv:hep-ph/0405247 [hep-ph].

[34] J. Pumplin et al., *New generation of parton distributions with uncertainties from global QCD analysis*, J. High Energy Phys. **0207** (2002) 012, arXiv:hep-ph/0201195 [hep-ph].

[35] S. Frixione and B. R. Webber, *The MC@NLO 3.2 event generator*, arXiv:hep-ph/0601192 [hep-ph].

[36] G. Corcella et al., *HERWIG 6: An Event generator for hadron emission reactions with interfering gluons (including supersymmetric processes)*, J. High Energy Phys. **0101** (2001) 010, arXiv:hep-ph/0011363 [hep-ph].

[37] J. Butterworth et al., *Multiparton interactions in photoproduction at HERA*, Z. Phys. C **72** (1996) 637–646.

[38] T. Gleisberg et al., *Event generation with SHERPA 1.1*, J. High Energy Phys. **0902** (2009) 007, arXiv:0811.4622 [hep-ph].

[39] J. Alwall, M. Herquet, F. Maltoni, O. Mattelaer, and T. Stelzer, *MadGraph 5 : Going Beyond*, J. High Energy Phys. **1106** (2011) 128.

[40] T. Sjostrand, S. Mrenna, and P. Z. Skands, *A Brief Introduction to PYTHIA 8.1*, Comput.Phys.Commun. **178** (2008) 852–867, arXiv:0710.3820 [hep-ph].

[41] M. Bähr et al., *Herwig++ Physics and Manual*, Eur. Phys. J. C **58** (2008) 639–707, arXiv:0803.0883 [hep-ph].

[42] W. Beenakker et al., *Squark and gluino production at hadron colliders*, Nucl. Phys. B **492** (1997) 51–103, arXiv:hep-ph/9610490 [hep-ph].

[43] A. Kulesza and L. Motyka, *Threshold resummation for squark-antisquark and gluino-pair production at the LHC*, Phys. Rev. Lett. **102** (2009) 111802, arXiv:0807.2405 [hep-ph].

[44] A. Kulesza and L. Motyka, *Soft gluon resummation for the production of gluino-gluino and squark-antisquark pairs at the LHC*, Phys. Rev. D **80** (2009) 095004, arXiv:0905.4749 [hep-ph].

[45] W. Beenakker et al., *Soft-gluon resummation for squark and gluino hadroproduction*, J. High Energy Phys. **0912** (2009) 041, arXiv:0909.4418 [hep-ph].

[46] W. Beenakker et al., *Squark and gluino hadroproduction*, Int. J. Mod. Phys. A **26** (2011) 2637–2664, arXiv:1105.1110 [hep-ph].

[47] M. Krämer et al., *Supersymmetry production cross sections in pp collisions at sqrts = 7 TeV*, arXiv:1206.2892 [hep-ph].

[48] ATLAS Collaboration, *The ATLAS Simulation Infrastructure*, Eur. Phys. J. C **70** (2010) 823–874, arXiv:1005.4568 [physics.ins-det].

[49] S. Agostinelli et al., *Geant4a simulation toolkit*, Nucl. Instrum. Meth. A **506** (2003) 250–303. http://www.sciencedirect.com/science/article/pii/S0168900203013688.

[50] D. Cavalli et al., "Performance of the atlas fast simulation atlfast." Internal report atl-phys-int-2007-005; atl-com-phys-2007-012, cern, geneva., 2007.

[51] M. Cacciari, G. Salam, and G. Soyez, *The anti-k_t jet clustering algorithm*, J. High Energy Phys. **0804** (2008) 063, arXiv:0802.1189 [hep-ph].

[52] M. Cacciari and G. Salam, *Dispelling the N3 myth for the kt jet-finder*, Phys. Lett. B **641** no. 1, (2006) 57 – 61.

[53] ATLAS Collaboration, *Jet energy measurement with the ATLAS detector in proton-proton collisions at $\sqrt{s} = 7$ TeV*, Eur.Phys.J.C **73** (2013) 2304, arXiv:1112.6426 [hep-ex].

[54] M. Cacciari and G. P. Salam, *Pileup subtraction using jet areas*, Phys.Lett. **B659** (2008) 119–126, arXiv:0707.1378 [hep-ph].

[55] ATLAS Collaboration, *Measurement of the b-tag Efficiency in a Sample of Jets Containing Muons with 5 fb^{-1} of Data from the ATLAS Detector*, ATLAS-CONF-2012-043 (2012). http://cdsweb.cern.ch/record/1435197.

[56] ATLAS Collaboration, *b-jet tagging calibration on c-jets containing D* mesons*, ATLAS-CONF-2012-039 (2012). http://cdsweb.cern.ch/record/1435193.

[57] ATLAS Collaboration, *Measurement of the Mistag Rate of b-tagging algorithms with 5 fb^{-1} of Data Collected by the ATLAS Detector*, ATLAS-CONF-2012-040 (2012). http://cdsweb.cern.ch/record/1435194.

[58] ATLAS Collaboration, *Electron performance measurements with the ATLAS detector using the 2010 LHC proton-proton collision data*, Eur. Phys. J. C **72** (2012) 1909, arXiv:1110.3174 [hep-ex].

[59] ATLAS Collaboration, *Measuring the b-tag efficiency in a ttbar sample with 4.7 fb^{-1} of data from the ATLAS detector*, ATLAS-CONF-2012-097 (2012). http://cdsweb.cern.ch/record/1460443.

[60] ATLAS Collaboration, *Single hadron response measurement and calorimeter jet energy scale uncertainty with the ATLAS detector at the LHC*, Eur.Phys.J.C **73** (2013) 2305, arXiv:1203.1302 [hep-ex].

[61] ATLAS Collaboration, *A study of heavy flavor quarks produced in association with top quark pairs at $\sqrt{s}$ = 7 TeV using the ATLAS detector*, arXiv:1304.6386 [hep-ex].

[62] CMS Collaboration, *First Measurement of Cross Section Ratio $\sigma(t\bar{t}b\bar{b})$ / $\sigma(t\bar{t}jj)$ in pp Collisions at 7 TeV*, 2013. http://cdsweb.cern.ch/record/1479150.

[63] M. Aliev et al., *Hadronic Top and Heavy quarks cross section calculator* , Comput. Phys. Commun. **182** (2011) 1034–1046, arXiv:1007.1327 [hep-ph].

[64] A. D. Martin et al., *Parton distributions for the LHC*, Eur. Phys. J. C **63** (2009) 189, arXiv:0901.0002 [hep-ph].

[65] A.D Martin et al., *Uncertainties on α_S in global PDF analyses and implications for predicted hadronic cross sections*, Eur. Phys. J. C **64** (2009) 653–680, arXiv:0905.3531 [hep-ph].

[66] M. Cacciari et al., *Top-pair production at hadron colliders with next-to-next-to-leading logarithmic soft-gluon resummation*, Phys. Lett. B **710** (2012) 612–622, arXiv:1111.5869 [hep-ph].

[67] M. Czakon and A. Mitov, *Top++: a program for the calculation of the top-pair cross-section at hadron colliders*, arXiv:1112.5675 [hep-ph].

[68] M. L. Mangano, M. Moretti, F. Piccinini, R. Pittau, and A. D. Polosa, *ALPGEN, a generator for hard multiparton processes in hadronic collisions*, J. High Energy Phys. **0307** (2003) 001, arXiv:hep-ph/0206293.

[69] ATLAS Collaboration, *Measurement of $t\bar{t}$ production with a veto on additional central jet activity in pp collisions at sqrt(s) = 7 TeV using the ATLAS detector*, Eur. Phys. J. C **72** (2012) 2043, arXiv:1203.5015 [hep-ex].

[70] ATLAS Collaboration, *Improved luminosity determination in pp collisions at sqrt(s) = 7 TeV using the ATLAS detector at the LHC*, arXiv:1302.4393 [hep-ex].

[71] A. L. Read, *Presentation of search results: the CL s technique*, Journal of Physics G: Nuclear and Particle Physics **28** no. 10, (2002) 2693. http://stacks.iop.org/0954-3899/28/i=10/a=313.

[72] G. Cowan et al., *Asymptotic formulae for likelihood-based tests of new physics*, Eur. Phys. J. C **71** (2011) 1554.

[73] ATLAS Collaboration, *Search for direct third generation squark pair production in final states with missing transverse momentum and two b-jets in $\sqrt{s}$ = 8 TeV pp collisions with the ATLAS detector.*, ATLAS-CONF-2013-053 (2013). http://cdsweb.cern.ch/record/1547570.

[74] ATLAS Collaboration, *Search for direct production of the top squark in the all-hadronic ttbar + etmiss final state in 21 fb^{-1} of p-pcollisions at $\sqrt{s}$ = 8 TeV with the ATLAS detector*, ATLAS-CONF-2013-024 (2013). http://cdsweb.cern.ch/record/1525880.

[75] ATLAS Collaboration, *Search for direct top squark pair production in final states with one isolated lepton, jets, and missing transverse momentum in $\sqrt{s}$ = 8 TeV pp collisions using 21 fb^{-1} of ATLAS data*, ATLAS-CONF-2013-037 (2013). http://cdsweb.cern.ch/record/1533431.

A Signal cross section upper limits

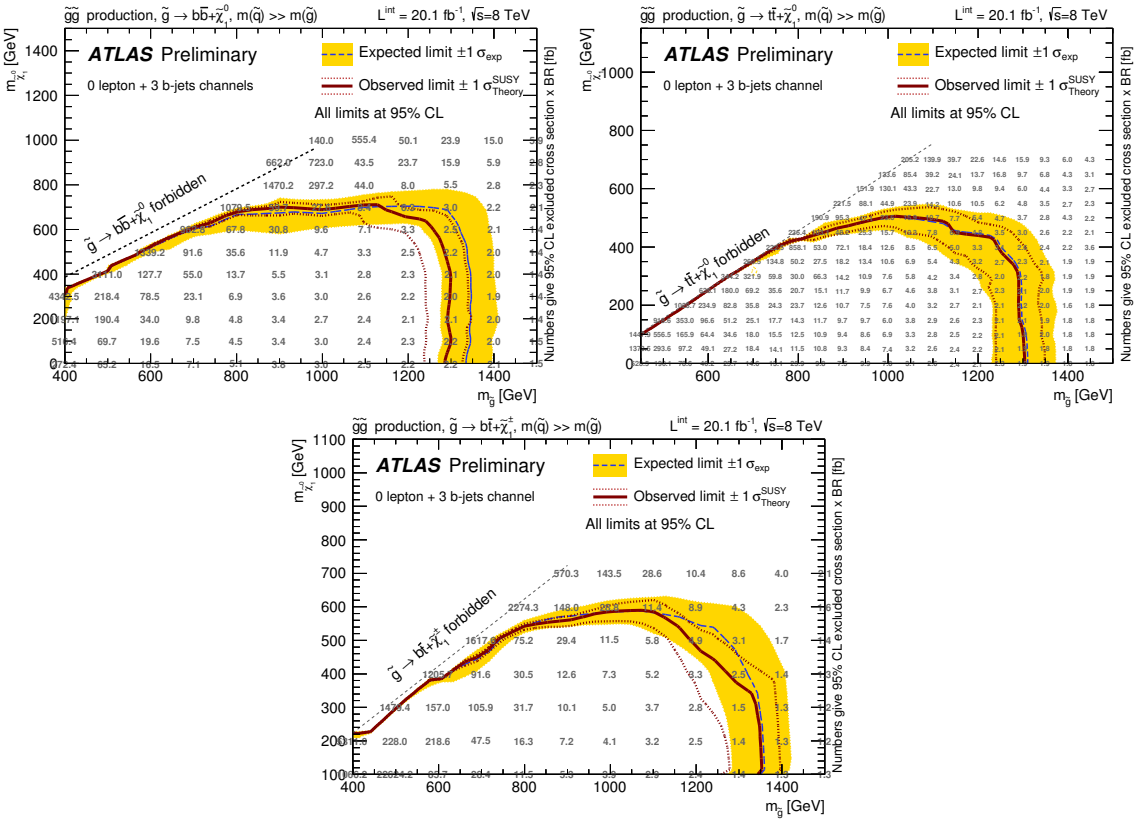

Figure 12: Upper cross section exclusion limits in the $(m_{\tilde{g}}, m_{\tilde{\chi}_1^0})$ plane for the Gbb (top left), Gbb (top right) and Gtb (bottom) models in the 0-lepton channel. The dashed blue and solid bold red lines show the 95% CL expected and observed limits respectively, including all uncertainties except the theoretical signal cross-section uncertainty. The shaded (yellow) bands around the expected limits show the impact of the experimental and background theoretical uncertainties while the dotted red lines show the impact on the observed limit of the variation of the nominal signal cross-section by 1σ of its theoretical uncertainty. The upper limit on the cross-section times branching ratio (in fb) is indicated for each model point.

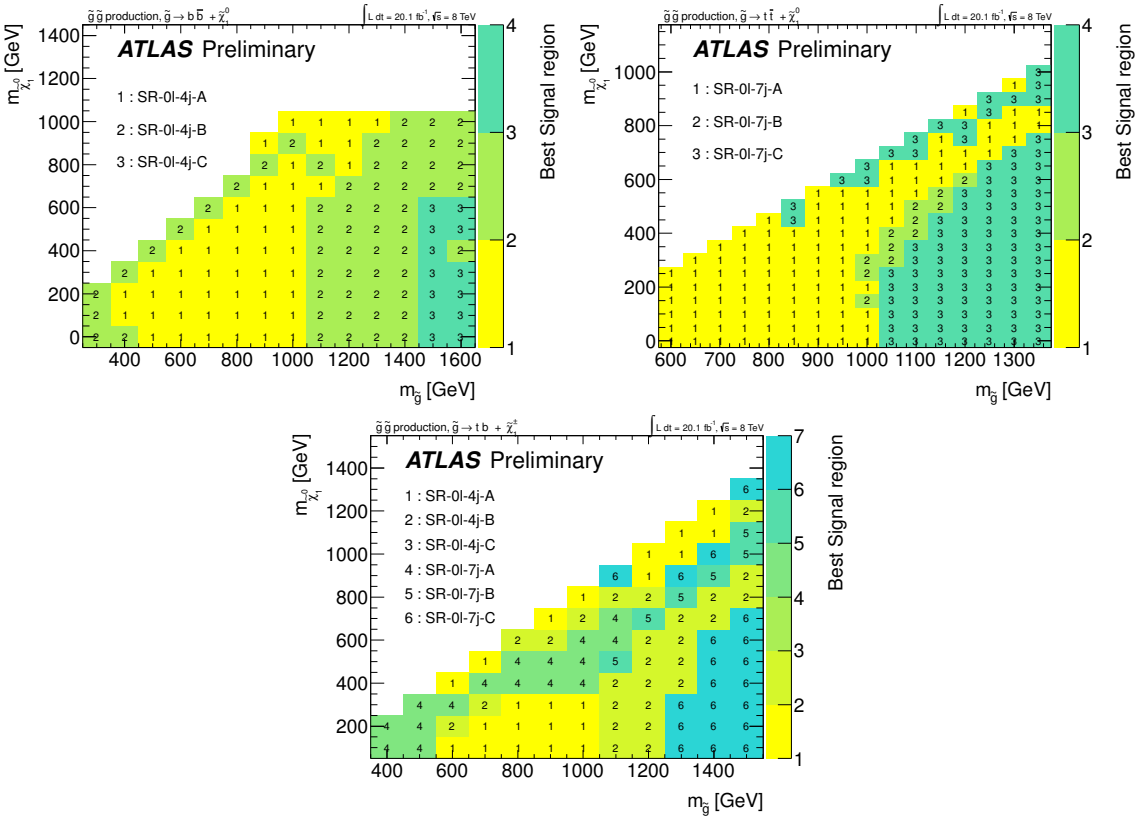

Figure 13: Signal regions yielding the best expected sensitivity, for each point of the $(m_{\tilde{g}}, m_{\tilde{\chi}_1^0})$ plane for the Gbb (top left), Gbb (top right) and Gtb (bottom) models in the 0-lepton channel.

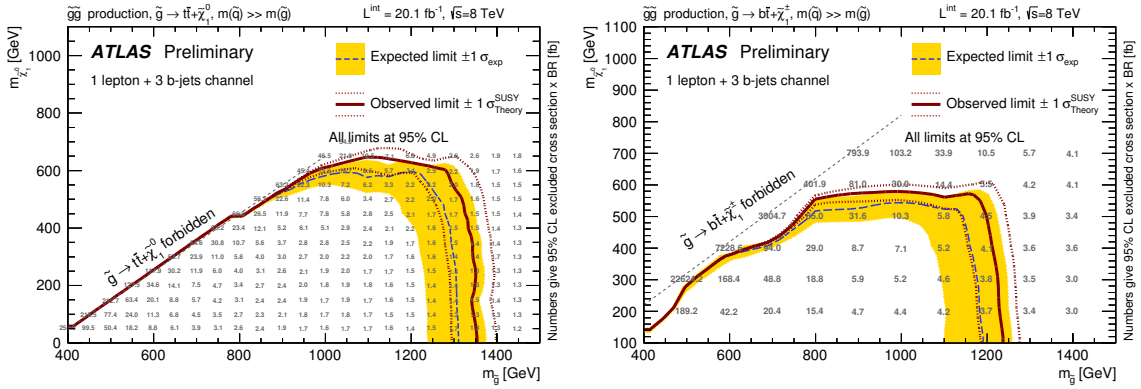

Figure 14: Upper cross section exclusion limits in the $(m_{\tilde{g}}, m_{\tilde{\chi}_1^0})$ plane for the Gtt (left) and Gtb (right) models in the 1-lepton channel. The dashed blue and solid bold red lines show the 95% CL expected and observed limits respectively, including all uncertainties except the theoretical signal cross-section uncertainty. The shaded (yellow) bands around the expected limits show the impact of the experimental and background theoretical uncertainties while the dotted red lines show the impact on the observed limit of the variation of the nominal signal cross-section by 1σ of its theoretical uncertainty. The upper limit on the cross-section times branching ratio (in fb) is indicated for each model point.

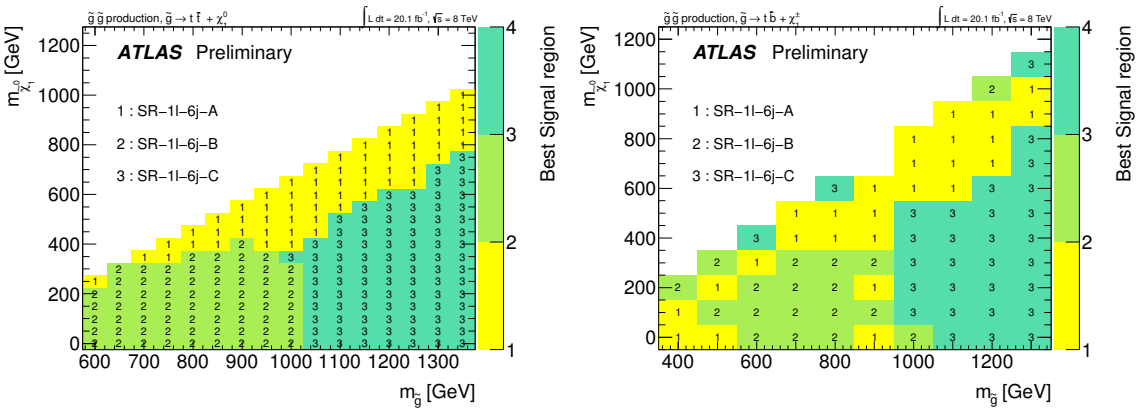

Figure 15: Signal regions yielding the best expected sensitivity, for each point of the $(m_{\tilde{g}}, m_{\tilde{\chi}_1^0})$ plane for the Gtt (left) and Gtb (right) models in the 1-lepton channel.

B Cut flow table

Process: Gbb model			
Point: $m_g = 1300$ GeV, $m_{\tilde{\chi}_1^0} = 100$ GeV			
Number of generated events: 100000			
Channel: 0-lepton			
Selection	Exp. event yield (Abs. Efficiency (%))		
Initial	39.0 (100.0%)		
Jet and Event cleaning	38.3 (98.2%)		
Cosmic muons rejection	38.3 (98.2%)		
≥ 4 jets ($p_{\mathrm{T}} > 30$ GeV)	37.2 (95.4%)		
1st jet $p_{\mathrm{T}} > 90$ GeV	37.2 (95.4%)		
$E_{\mathrm{T}}^{\mathrm{miss}} > 150$ GeV	34.6 (88.7%)		
Electron veto	34.6 (88.7%)		
Muon veto	34.4 (88.2%)		
$\Delta\phi_{\mathrm{min}}^{4j} > 0.5$	22.8 (58.5%)		
$E_{\mathrm{T}}^{\mathrm{miss}}/m_{\mathrm{eff}}^{\mathrm{4j}} > 0.2$	18.0 (46.2%)		
	SR-0l-4j-A	SR-0l-4j-B	SR-0l-4j-C
≥ 4 jets with $p_{\mathrm{T}} > 30-50-50$ GeV	18.0 (46.2%)	16.7 (42.8%)	16.7 (42.8%)
≥ 3 b-jets with $p_{\mathrm{T}} > 30-50-50$ GeV	8.0 (20.5%)	7.0 (17.9%)	7.0 (17.9%)
$E_{\mathrm{T}}^{\mathrm{miss}} > 200-350-250$ GeV	8.0 (20.5%)	6.3 (16.2%)	6.8 (17.4%)
$m_{\mathrm{eff}}^{\mathrm{4j}} > 1000-1100-1300$ GeV	7.9 (20.3%)	6.2 (15.9%)	6.2 (15.9%)
$E_{\mathrm{T}}^{\mathrm{miss}}/\sqrt{H_{\mathrm{T}}^{\mathrm{4j}}} > 16-0-0$ GeV$^{\frac{1}{2}}$	4.2 (10.8%)	-	-

Table 6: Cut flow table for the number of expected events in the various 0-lepton channel signal regions for one benchmark point in the Gbb model. All numbers are normalised to 20.1 fb^{-1}. The absolute efficiency in % is provided in parenthesis. The signal samples are generated with `MADGRAPH 5.1.4.8` interfaced to `PYTHIA 6.426` in order to ensure an accurate treatment of the initial-state radiation (ISR), and with the PDF set `CTEQ6L1`.

Process: Gtt model			
Point: $m_g = 1300$ GeV, $m_{\tilde{\chi}_1^0} = 100$ GeV			
Number of generated events: 100000			
Channel: 0-lepton			
Selection	Exp. event yield (Abs. Efficiency (%))		
Initial	39.0 (100.0%)		
Jet and Event cleaning	38.4 (98.4%)		
Cosmic muons rejection	38.1 (97.2%)		
≥ 4 jets ($p_{\mathrm{T}} > 30$ GeV)	37.8 (96.9%)		
1st jet $p_{\mathrm{T}} > 90$ GeV	37.8 (96.9%)		
$E_{\mathrm{T}}^{\mathrm{miss}} > 150$ GeV	34.4 (88.3%)		
Electron veto	23.3 (59.7%)		
Muon veto	17.9 (45.9%)		
$\Delta\phi_{\mathrm{min}}^{4j} > 0.5$	11.7 (30.0%)		
$E_{\mathrm{T}}^{\mathrm{miss}}/m_{\mathrm{eff}}^{\mathrm{4j}} > 0.2$	10.1 (25.9%)		
≥ 7 jets ($p_{\mathrm{T}} > 30$ GeV)	9.6 (24.6%)		
≥ 3 b-jets ($p_{\mathrm{T}} > 30$ GeV)	4.5 (11.5%)		
	SR-0l-7j-A	SR-0l-7j-B	SR-0l-7j-C
$E_{\mathrm{T}}^{\mathrm{miss}} > 200 - 350 - 250$ GeV	4.4 (11.3%)	3.6 (9.2%)	4.2 (10.8%)
$m_{\mathrm{eff}}^{\mathrm{incl}} > 1000 - 1000 - 1500$ GeV	4.4 (11.3%)	3.6 (9.2%)	3.7 (9.5%)

Table 7: Cut flow table for the number of expected events in the various 0-lepton channel signal regions for one benchmark point in the Gtt model. All numbers are normalised to 20.1 fb^{-1}. The absolute efficiency in % is provided in parenthesis. The signal samples are generated with `HERWIG++ 2.5.2` and with the PDF set `CTEQ6L1`.

Process: Gtt model			
Point: $m_g = 1300$ GeV, $m_{\tilde{\chi}_1^0} = 100$ GeV			
Number of generated events: 100000			
Channel: 1-lepton			
Selection	Exp. event yield (Abs. Efficiency (%))		
Initial	39.0 (100.0%)		
Jet and Event cleaning	38.4 (98.4%)		
Cosmic muons rejection	38.1 (97.2%)		
≥ 4 jets ($p_{\mathrm{T}} > 30$ GeV)	37.8 (96.9%)		
1st jet $p_{\mathrm{T}} > 90$ GeV	37.8 (96.8%)		
$E_{\mathrm{T}}^{\mathrm{miss}} > 150$ GeV	34.4 (88.3%)		
≥ 1 signal lepton	15.9 (40.9%)		
≥ 6 jets ($p_{\mathrm{T}} > 30$ GeV)	14.6 (37.3%)		
≥ 3 b-jets	5.6 (14.3%)		
	SR-1l-6j-A	SR-1l-6j-B	SR-1l-6j-C
$m_{\mathrm{T}} > 140 - 140 - 160$ GeV	4.4 (11.3%)	4.4 (11.3%)	4.2 (10.7%)
$E_{\mathrm{T}}^{\mathrm{miss}} > 175 - 225 - 275$ GeV	4.3 (10.9%)	3.9 (10.0%)	3.4 (8.8%)
$E_{\mathrm{T}}^{\mathrm{miss}} / \sqrt{H_{\mathrm{T}}^{\mathrm{incl}}} > 5$ GeV$^{1/2}$	4.2 (10.8%)	3.9 (10.0%)	3.4 (8.8%)
$m_{\mathrm{eff}}^{\mathrm{incl}} > 700 - 800 - 900$ GeV	4.2 (10.8%)	3.9 (10.0%)	3.4 (8.8%)

Table 8: Cut flow table for the number of expected events in the various 1-lepton channel signal regions for one benchmark point in the Gtt model. All numbers are normalised to 20.1 fb^{-1}. The absolute efficiency in % is provided in parenthesis. The signal samples are generated with `HERWIG++ 2.5.2` and with the PDF set `CTEQ6L1`.